


Cite this: *RSC Adv.*, 2023, 13, 12184

Novel 4-thiophenyl-pyrazole, pyridine, and pyrimidine derivatives as potential antitumor candidates targeting both EGFR and VEGFR-2; design, synthesis, biological evaluations, and *in silico* studies†

Samia M. Al-Muntaser,^{‡a} Ahmed A. Al-Karmalawy,^{ID ‡*b} Abeer M. El-Naggar,^{ID a} Ali Khalil Ali,^{ID a} Nour E. A. Abd El-Sattar^{ID a} and Eslam M. Abbass^{ID *a}

In this article, we continued our previous effort to develop new selective anticancer candidates based on the basic pharmacophoric requirements of both EGFR and VEGFR-2 inhibitors. Therefore, twenty-two novel 4-thiophenyl-pyrazole, pyridine, and pyrimidine derivatives were designed and examined as dual EGFR/VEGFR-2 inhibitors. Besides, the previously reported antimicrobial activities of the aforementioned nuclei motivated us to screen their antibacterial and antifungal activities as well. First, the antitumor activities of the newly synthesized derivatives were evaluated against two cancer cell lines (HepG-2 and MCF-7). Notably, compounds **2a**, **6a**, **7a**, **10b**, **15a**, and **18a** exhibited superior anticancer activities against both HepG-2 and MCF-7 cancer cell lines. These candidates were selected to further evaluate their anti-EGFR and anti-VEGFR-2 potentialities which were found to be very promising compared to erlotinib and sorafenib, respectively. Both **10b** and **2a** derivatives achieved better dual EGFR/VEGFR-2 inhibition with IC₅₀ values of 0.161 and 0.141 μM and 0.209 and 0.195 μM, respectively. Moreover, the most active **10b** was selected to evaluate the exact phase of cell cycle arrest and to investigate the exact mechanism of cancer cell death whether it be due to apoptosis or necrosis. On the other hand, all the synthesized compounds were tested against Gram-positive bacteria such as *S. aureus* and *B. subtilis* as well as Gram-negative bacteria such as *E. coli* and *P. aeruginosa*. Also, the antifungal activity was investigated against *C. albicans* and *A. flavus* strains. The findings of the antimicrobial tests revealed that most of the investigated compounds exhibited strong to moderate antibacterial and antifungal effects. Furthermore, to understand the pattern by which the investigated compounds bound to the active site, all the newly synthesized candidates were subjected to two different docking processes into the EGFR and VEGFR-2 binding sites. Besides, we tried to correlate compound **10b** and the reference drugs (erlotinib and sorafenib) through DFT calculations. Finally, following the biological data of the new pyrazole, pyridine, and pyrimidine derivatives as anticancer and antimicrobial candidates, we concluded a very interesting SAR for further optimization.

Received 19th January 2023
Accepted 11th April 2023

DOI: 10.1039/d3ra00416c

rsc.li/rsc-advances

1. Introduction

One of the most dangerous diseases in the world that threatens human life is cancer. It is considered the second driving cause

of death in the world.^{1,2} According to global statistics, cancer is considered one of the primary causes of death worldwide.^{3,4}

Nowadays, medicinal chemists are requested to find out effective and specific chemotherapeutic agents.^{5,6} Such drugs are designed for inhibiting cancer cell growth by way of interacting with particular molecular targets resulting in substantial harm to the cancerous cells.^{7,8} However, some problems like resistance, delivery, and/or selectivity may diminish the process of drug development.^{9,10} Therefore, there is a great interest to understand the cellular and molecular pathways that contribute to the process of cancer initiation and/or spread.^{11,12}

Protein kinases (PKs) constitute crucial protein families in the process of diverse disease propagation such as cancer, diabetes, and/or inflammation. Therefore, they constitute a very

^aDepartment of Chemistry, Faculty of Science, Ain Shams University, Abbassiya 11566, Cairo, Egypt. E-mail: eslammorad@sci.asu.edu.eg

^bPharmaceutical Chemistry Department, Faculty of Pharmacy, Ahram Canadian University, 6th of October City, Giza 12566, Egypt. E-mail: akarmalawy@acu.edu.eg

† Electronic supplementary information (ESI) available: Elemental analysis tables, IR, NMR, and mass spectra of all target compounds. See DOI: <https://doi.org/10.1039/d3ra00416c>

‡ Equal contribution.



promising target for new drug discovery due to their prominent roles in several cellular functions like apoptosis, cell cycle, DNA damage/repair, and metabolism.^{13–16}

Many types of tumors such as colon, breast, and ovarian subtypes resulted from the overexpression of EGFR (epidermal growth factor receptor). EGFR is a transmembrane PK receptor that is responsible for cell proliferation and/or apoptosis through different signal transduction pathways. It was recorded to be involved in the process of angiogenesis which increases the proliferation of tumor cells, invasiveness, and metastasis.¹⁷ EGFR inhibitors (*e.g.* erlotinib)¹⁸ are one of the most important FDA-approved drugs for cancer treatment, Fig. 1.

Besides, EGFR stimulation results in increasing the expression of VEGF (vascular endothelial growth factor) which is the main factor that is responsible for tumor angiogenesis after its binding to VEGFR-2 (vascular endothelial growth factor receptor-2).¹⁹ Therefore, FDA-approved VEGFR-2 inhibitors (*e.g.* sorafenib)²⁰ are considered potential anticancer drugs, Fig. 1.

Due to the close relationship between the two previously discussed pathways, we can confirm that EGFR blocking will result in decreasing the endothelial expression of VEGF. Also, VEGFR-2 inhibition will potentiate the anticancer activity of EGFR inhibitors.²¹ Based on the above, the dual inhibition of EGFR and VEGFR-2 represents a very promising protocol for cancer treatment.²² One of the most potent dual EGFR/VEGFR-2 inhibitors is vandetanib (Fig. 1) which is an FDA-approved drug against thyroid cancer.²³

According to Fig. 1, we can observe the common and greatly similar pharmacophoric features of EGFR and/or VEGFR-2 inhibitors. Both types require the presence of four

pharmacophores which are the hydrophobic head, H-bond donor (for EGFR) or H-bond donor and acceptor (for VEGFR-2), spacer flat heteroaromatic ring, and hydrophobic tail.^{14,24,25}

Pyrazole, pyridine, and pyrimidine systems constitute very promising scaffolds for many anticancer agents. They were previously reported as potential EGFRIs,^{26,27} VEGFR-2Is,^{28,29} and/or dual EGFR/VEGFR-2 inhibitors.^{30,31} Based on the aforementioned facts, we aimed to develop novel 4-thiophenyl-pyrazole, pyridine, and pyrimidine derivatives as promising inhibitors against both EGFR and VEGFR-2. On the other hand, the previously mentioned moieties showed apparent antimicrobial activities^{32,33} which encourages us to screen the antibacterial and antifungal activities of the newly designed targets.

1.1. Rationale and work design

Based on the above, we designed and introduced novel 4-thiophenyl-pyrazole, pyridine, and pyrimidine derivatives as potential antitumor candidates targeting both EGFR and VEGFR-2 receptors.

Briefly, the principal pharmacophoric features of EGFR inhibitors (Fig. 2) were identified as follows:²

- (a) Hydrophobic head to bind the hydrophobic region I.
- (b) H-bond donor in the spacer region.
- (c) Flat heteroaromatic ring to bind the adenine binding pocket.
- (d) Hydrophobic tail to bind the hydrophobic region I.

However, the pharmacophoric features of VEGFR-2 inhibitors (Fig. 2) were identified as:³⁴

- (a) Flat aromatic ring to occupy the hinge region.

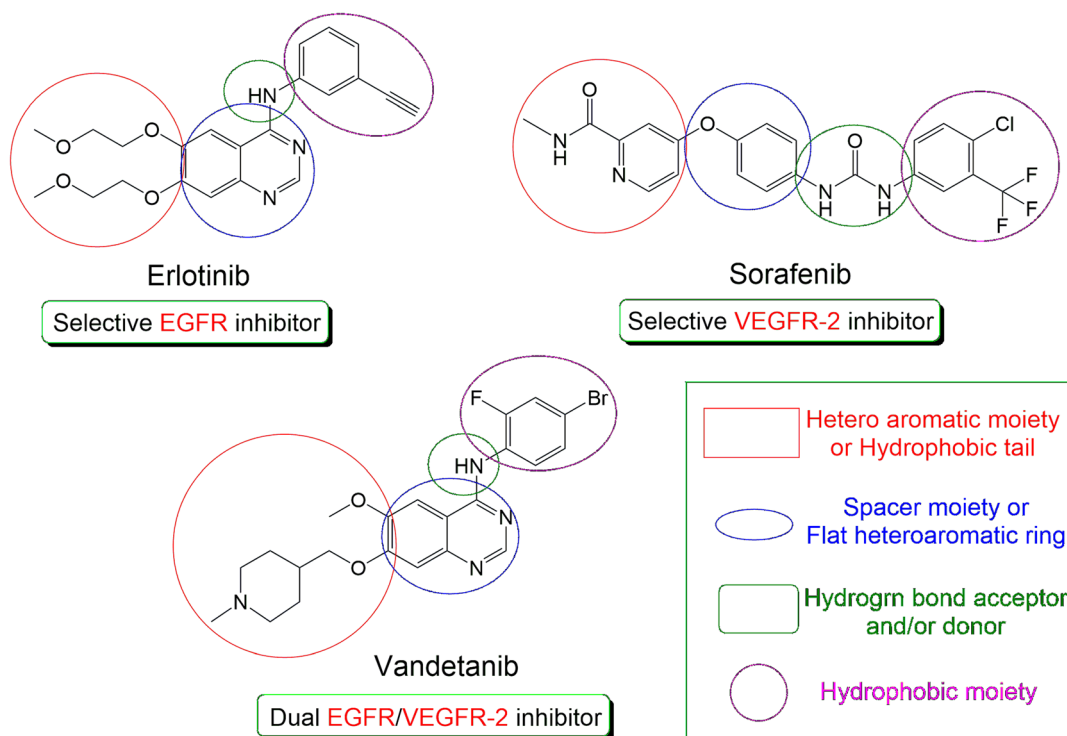


Fig. 1 The common pharmacophoric features of the FDA-approved drugs (erlotinib, sorafenib, and vandetanib).

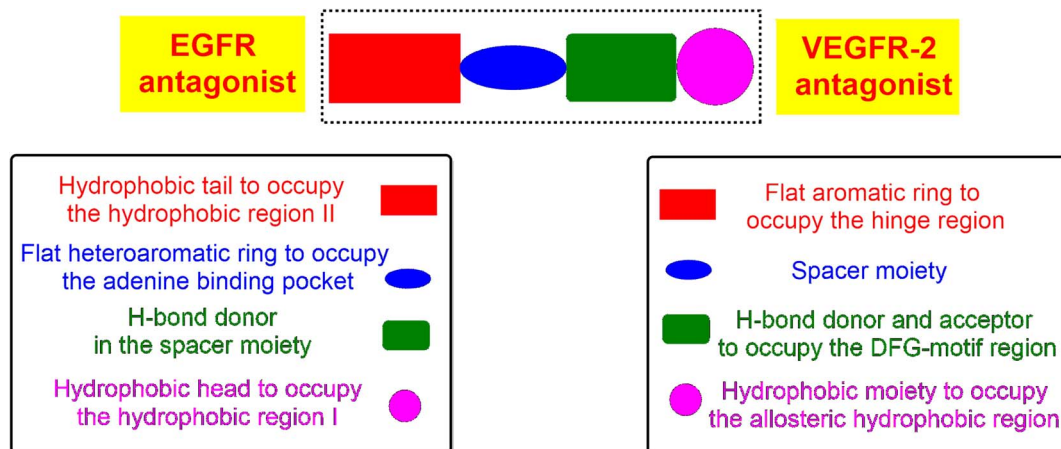


Fig. 2 Pharmacophoric features of both EGFR and VEGFR-2 antagonists.

(b) Spacer moiety.

(c) Both the H-bond donor and acceptor to bind the DFG motif.

(d) Hydrophobic moiety to bind the allosteric hydrophobic region.

Therefore, the new design is based on the introduction of the thiophene ring to act as a hydrophobic tail and bind the hydrophobic region II of EGFR or the hinge region of VEGFR-2. Besides, the pyridine or pyrazole moiety to bind the adenine binding pocket of EGFR or to act as a spacer for the VEGFR-2 receptor. Moreover, different functional groups were introduced as H-bond donors and/or acceptors to form H-bonds in the spacer region of EGFR or the DFG-motif region of VEGFR-2. Finally, a *p*-hydroxyphenyl ring was added to occupy the hydrophobic region I of EGFR or the allosteric hydrophobic region of VEGFR-2.

Accordingly, the main aim of this new design is to target both EGFR and VEGFR-2 receptors even if not all the pharmacophoric features are present typically in the new candidates. The atypical design of some new derivatives may give them adequate flexibility to bind both receptors which may be advantageous.

On the other hand, the previously reported antibacterial and/or antifungal activities of the pyrazole, pyridine, and pyrimidine derivatives motivated us to further screen the antibacterial and antifungal activities of the newly synthesized candidates.

2. Results and discussion

2.1. Chemistry

The α , β unsaturated ketone derivatives are highly reactive molecules that contain two reactive centers to be used as a bidentate reagent in the synthesis of different heterocyclic moieties.^{34,35} On the other hand, active methylene and cyclic active methylene compounds like dimedone, 1,3-indandione, and its derivatives were approved for their anticancer activities and were also used as key starting materials for the synthesis of biologically active heterocyclic compounds.^{36,37}

Thus, we synthesized a polarized system as 1-(aryl)-3-(thiophen-2-yl)prop-2-en-1-one “chalcone”, and then accomplished by ring closure to afford novel heterocyclic compounds (pyridine and pyrazole). Claisen–Schmidt condensation^{38,39} of substituted ketone derivatives with thiophene-2-carboxaldehyde afforded chalcones **1a** and **1b** (Scheme 1).

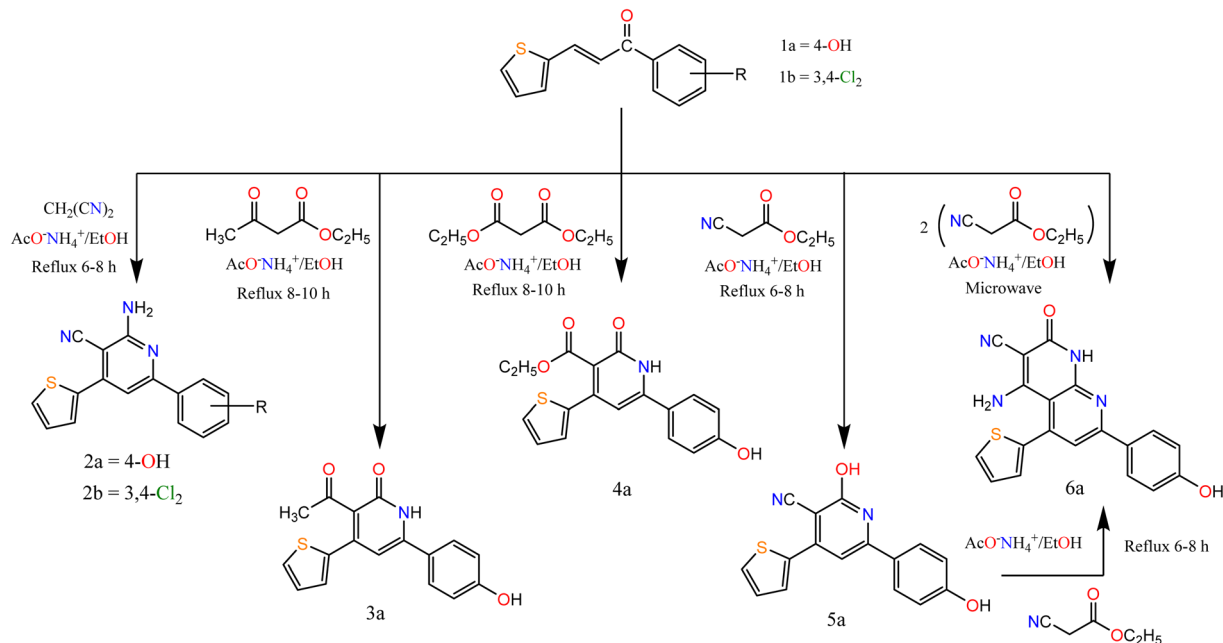
According to the previously reported methods, the derivatives were prepared at a high yield. The chalcone derivatives and suitable nucleophile compounds were heated under reflux conditions and utilized for the synthesis of various pyrimidine and pyrazole derivatives. All the target compounds **1a–20a** were characterized using spectral data such as ¹H NMR, mass, and IR spectroscopy. Moreover, the purity of the previously mentioned derivatives was confirmed by elemental analyses as depicted in the ESI.†

The spectral data of chalcone **1b** laid a strong foundation for a confirmation of the chemical structure and stereochemistry of **1b**. The IR spectrum exhibited an absorption band at 1655 cm^{−1} characteristic of functionalities of C=O. Moreover, the ¹H NMR spectrum of chalcone **1b** indicated the presence of two doublets at 7.57 and 7.92 ppm corresponding to β and α protons of C=C, respectively, with $J = 14.8$ Hz.

In this paper, we study the behavior of chalcones **1a**, **1b** towards some C- and N-nucleophilic reagents. So, we synthesized new heterocyclic compounds by refluxing chalcone **1a** and or **1b** in ethanol in the presence of ammonium acetate with malononitrile, ethyl acetoacetate, and diethyl malonate afford the pyridine derivatives **2a–6a** respectively. In the case of ethyl cyanoacetate addition of one molecule afforded compound **5a** while the addition of two molecules afforded compound **6a**. Their structures were confirmed by recording their spectral data. For compounds **2a** and **2b**. The IR spectrum showed bands at the range 3223–3362 and 2200–2213 cm^{−1} attributed to NH₂ and CN groups respectively. The ¹H NMR spectra of compounds **2a** and **2b** exhibited a singlet signal at δ 7.15 and 6.91 attributed to NH₂ protons, respectively.

However, the IR spectrum of compound **3a** showed bands at 3107 and 1695 cm^{−1} attributed to NH and CO groups



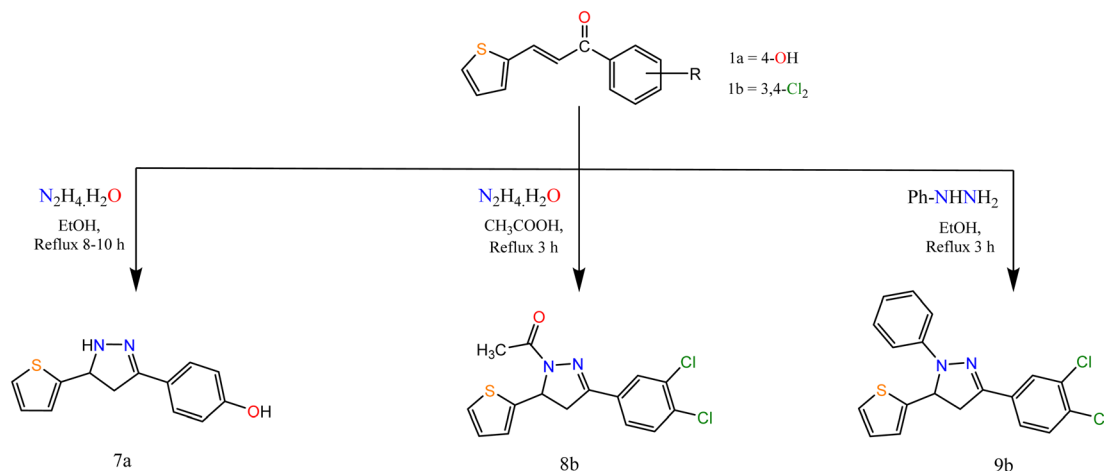


Scheme 1 Synthesis of the target compounds (2a, b), 3a, 4a, 5a, and 6a.

respectively. The ^1H NMR spectrum exhibited a singlet at δ 2.50 and 9.86 ppm, attributed to $\text{CH}_3\text{-CO}$ and OH protons, respectively. For compound 4a its IR spectra exhibited bands at 3170, 1725, and 1675 cm^{-1} attributed to NH and 2 CO groups. The ^1H NMR spectrum exhibited signals at δ 1.11, 3.91, and 7.19 ppm, attributed to CH_3 , CH_2 , and NH proton, respectively. For compound 5a its IR spectra exhibited bands at 3301, 2216, and 1636 cm^{-1} attributed to OH, CN, and $\text{C}=\text{N}$ groups, respectively. The ^1H NMR spectrum exhibited a singlet at δ 10.22, and 12.48 ppm, attributed to two OH protons. The spectral data of compound 6a confirmed the expected structure. IR spectra exhibited bands at 3369, 2217, and 1683 cm^{-1} attributed to NH, CN, and CO groups. The ^1H NMR spectrum exhibited a singlet at δ 6.47 and 9.81 ppm, attributed to NH_2 , and NH proton, respectively.

Moreover, the reaction of α,β -unsaturated ketones with hydrazine hydrate and its derivatives (Scheme 2) for synthesis, pyrazolines is one of the most convenient methods. Pyrazoline derivatives 7a–9b were synthesized by the reaction of chalcones 1a and/or 1b with hydrazine hydrate in ethanol, in glacial acetic acid and phenylhydrazine, respectively *via* aza Michael addition of hydrazine on chalcone 1b, followed by a 5-*exo*-trig ring cyclization and dehydration. Elemental analyses, IR, and ^1H NMR spectra supported the structure confirmation of compounds 7a–9b (Scheme 2).

The IR spectra of compounds 7a–9b showed bands at the range $1606\text{--}1636\text{ cm}^{-1}$ that account for the formation of the $\text{C}=\text{N}$ bond. In addition, compound 8b showed a band at 1667 cm^{-1} attributed to CO. The appearance of CH_2 proton at 2.82, 3.27, 3.24 ppm in the ^1H NMR spectra of compounds 7a–



Scheme 2 Synthesis of the target compounds 7a, 8b, and 9b.

9b respectively, confirmed the formation of the pyrazole ring, in addition to the appearance of signals at δ 5.05, 5.84 and 5.86 for compounds **7a–9b**, respectively attributed to CH proton of pyrazole ring. Also, compound **8b** showed a singlet signal at 2.48 ppm accounts for the CH₃ protons.

Similarly, the reaction of chalcones **1a**, **b** with thiosemicarbazide in two different conditions afforded pyrazole carbothioamide derivative, the first condition is refluxing of chalcone **1a** in ethanolic solution in the presence of a catalytic amount of acetic acid afforded compound **10a** the second condition is refluxing of chalcone **1b** in ethanolic sodium hydroxide solution afforded compound **10b** (Scheme 3).

Alkylation of both compounds **10a** and **10b** by 2,3-dichloroquinoxalin and phenacyl bromide afforded pyrazole derivatives **12a** and **12b**, respectively. Refluxing of chalcone **1a** with guanidine hydrochloride in ethanolic sodium hydroxide solution afforded compound **11a** which condensed with salicylaldehyde in ethanol with a catalytic amount of piperidine afforded pyrimidine derivative **13a** (Scheme 3).

The IR spectra of compounds **10a**, **10b**, and **11a** showed bands at the range 3145–3343 cm^{−1} that account for the presence of NH₂ and showed bands at the range 1636–1639 cm^{−1} that account for the formation of C=N. In addition, compound **12b** showed bands at 1668 and 2849 cm^{−1} attributed to CO and CH-aliphatic, respectively. The ¹H NMR spectra of compounds **10a** and **11a** showed the appearance of singlet signals at 6.88, 6.99, and 7.65 ppm, attributed to CH protons of pyrazole and

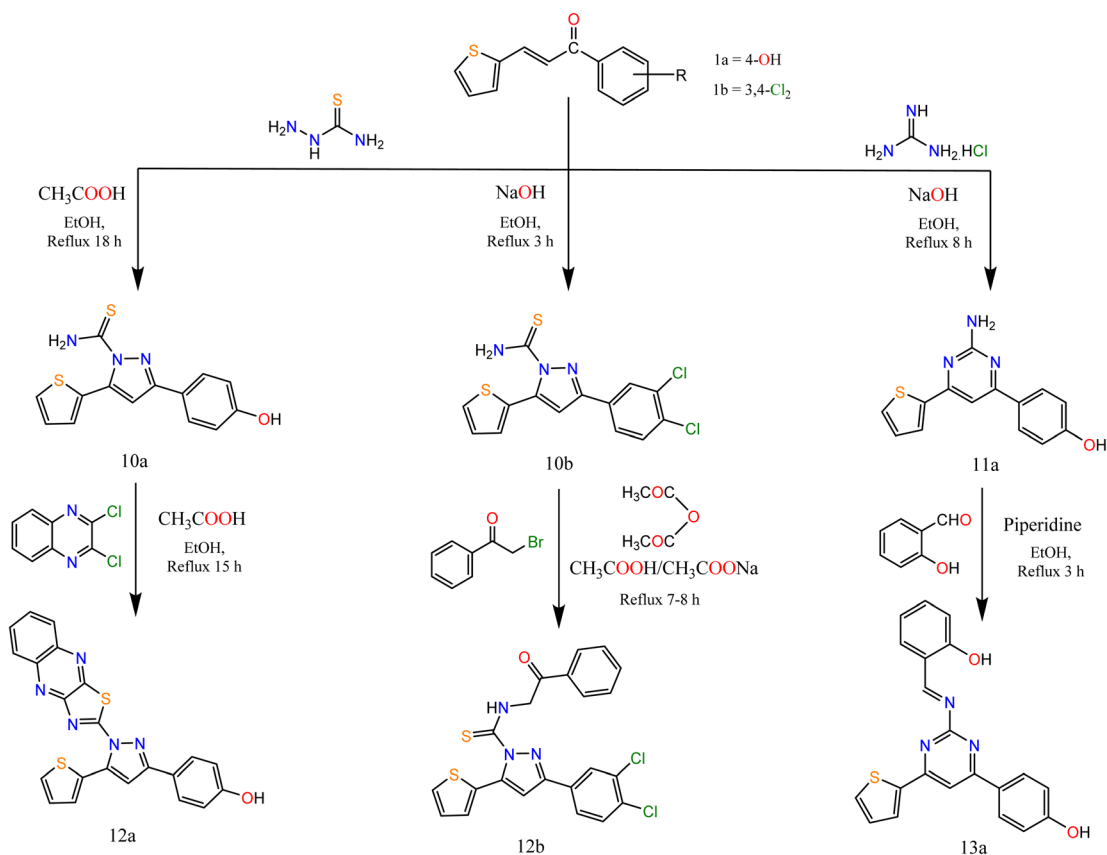
pyrimidine rings, respectively. In addition, compound **12b** showed a singlet signal at 4.82 attributed to CH₂ protons. Compound **13a** showed singlet signals at 7.51 and 7.56 attributed to CH of pyrimidine and CH=N.

Furthermore, to study the reactivity of pyrazole ring towards the electrophilic reagents as **7a** with phenyl isothiocyanate, ethyl chloroacetate, and 2-chloro-*N*-(4-sulfamoylphenyl)acetamide in different conditions afforded pyrazole derivatives **14a–16a** (Scheme 4).

The spectral data were in agreement with the predicted structure of the compounds. For compound **15a**, the IR spectrum showed bands at 1731 cm^{−1} attributed to the CO group. Its ¹H NMR exhibited triplet and quartet signals at 1.02 and 4.09 ppm attributed to CH₃ and CH₂ protons. For compound **16a**, the IR spectrum showed bands at 1694 cm^{−1} attributed to the CO group. Its ¹H NMR exhibited signals at 5.15 ppm attributed to CH₂ protons of the acetamide group.

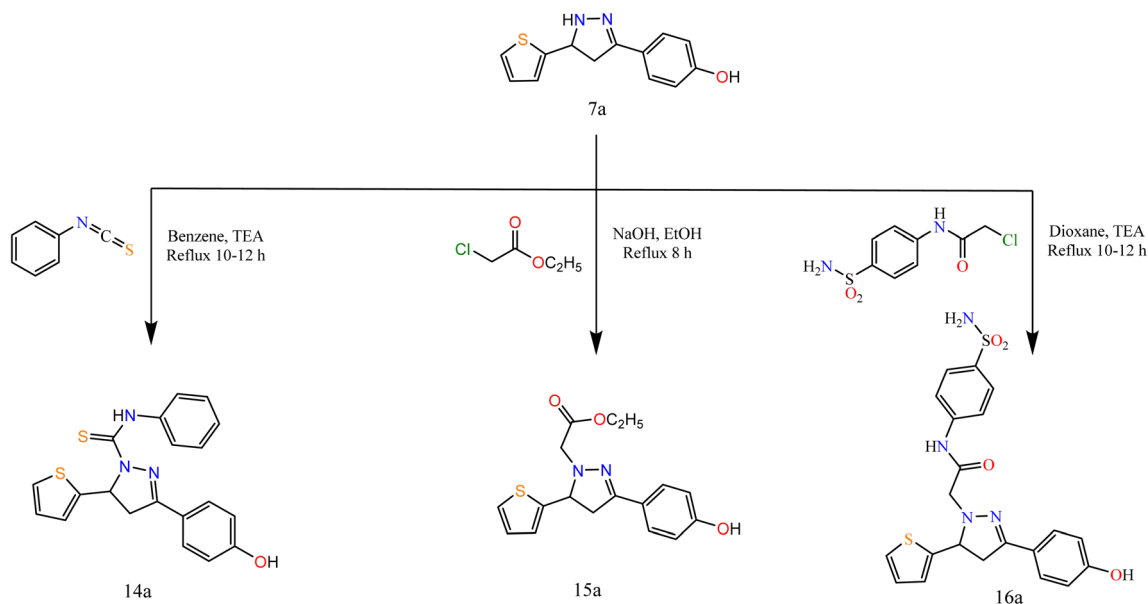
On the other hand, in extension to our previous work on the PTC alkylation of 1,3-disubstituted-2-pyrazolin-5-ones^{40,41} we have studied here the reactivity of pyrazole derivative towards PTC alkylation and acylation in the presence or absence of CS₂.

Alkylation of pyrazole derivative (**7a**) by ethylchloroacetate, benzoyl chloride, chloroacetic acid, and chloroacetyl chloride in the presence of carbon disulfide under liquid/solid PTC reaction conditions afforded pyrazole-1-carbonothioyl **17a–20a** (Scheme 5).

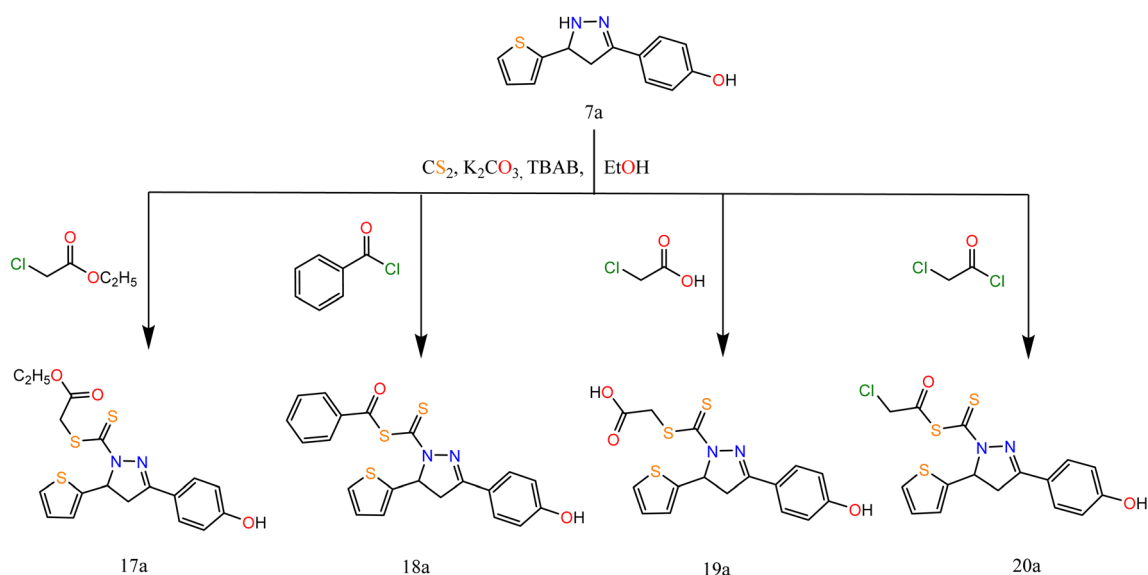


Scheme 3 Synthesis of the target compounds **10a**, **10b**, **11a**, **12a**, **12b**, and **13a**.





Scheme 4 Synthesis of the target compounds 14a, 15a, and 16a.



Scheme 5 Synthesis of the target compounds 17a, 18a, 19a, and 20a.

The IR spectra of 17a–20a showed bands at 1696, (1696, 1736), 1692, and (1746, 1694) cm^{−1} attributed to CO groups, respectively. For more conformation to the predicted structure. The ¹H NMR of 17a exhibited signals at 4.06 ppm attributed to CH₂ protons of the ester group. The CH₂ group of acid present in compound 19a exhibited a singlet signal at 3.60 ppm. However, the CH₂ of acetyl chloride in compound 20a exhibited a singlet signal at 4.35 ppm.

The reaction proceeds *via* the nucleophilic addition of pyrazole at N[−] to CS₂ followed by simultaneous *N*-alkylation of the intermediate thiocarbanic acid. The suggested mechanism is represented in the ESI.†

2.2. Biological evaluations

2.2.1. Anti-proliferative activities. The antitumor activities of the newly synthesized derivatives against two cancer cell lines (HepG-2 and MCF-7), Table 1, based on their main nuclei (pyrazole-based, pyridine-based, and pyrimidine-based moieties) showed the following interesting results:

(a) Pyrazole-based moieties:

• Dihydropyrazole derivatives were more active than pyrazole ones against the two cancer cell lines. Dihydropyrazole candidates which do not contain *N*-substitution like 7a showed very strong activities against both HepG-2 and MCF-7 more than the *N*-substituted dihydropyrazoles.

Table 1 Anti-proliferative activities of the newly designed 4-thio-phenyl-pyrazole, pyridine, and pyrimidine derivatives against HepG-2 and MCF-7 cancer cell lines

Comp.	Cell lines (IC ₅₀ μM)	
	HepG-2	MCF-7
1a	87.56 ± 4.2	82.45 ± 4.2
1b	84.16 ± 4.2	>100
2a	8.42 ± 0.6	9.59 ± 0.8
2b	59.47 ± 3.1	55.46 ± 3.2
3a	53.21 ± 3.1	48.35 ± 2.7
4a	44.45 ± 2.6	41.22 ± 2.4
5a	43.03 ± 2.5	38.37 ± 2.5
6a	16.24 ± 1.3	19.12 ± 1.6
7a	8.13 ± 0.6	3.54 ± 0.2
8b	74.28 ± 3.5	72.64 ± 3.9
9b	48.11 ± 2.7	67.33 ± 3.7
10a	39.07 ± 2.4	23.72 ± 1.7
10b	13.81 ± 1.1	23.24 ± 1.8
11a	52.94 ± 2.9	61.08 ± 3.4
12a	74.73 ± 3.9	65.03 ± 3.6
12b	29.20 ± 2.1	35.95 ± 2.3
13a	34.76 ± 2.3	42.75 ± 2.6
14a	69.20 ± 3.6	54.81 ± 3.1
15a	21.38 ± 1.5	9.48 ± 0.7
16a	34.53 ± 2.2	29.06 ± 2.0
17a	62.41 ± 3.3	36.87 ± 2.2
18a	12.94 ± 1.0	6.92 ± 0.5
19a	28.20 ± 1.9	14.69 ± 1.2
20a	67.41 ± 3.5	56.19 ± 3.3
DOX	4.50 ± 0.2	4.17 ± 0.2

• *N*-Substituted dihydropyrazole with CH₂-CO-attracting group like **15a** showed very strong activity against MCF-7 and moderate activity against HepG-2 while *N*-substituted dihydropyrazole with CH₂-CO-donating group like **16a** represented moderate activities against both cell lines.

• On the other hand, *N*-substituted dihydropyrazole with CS-S-G side chains as in compounds **17a–20a** have higher activities on the MCF-7 than the HepG-2 cell line. They showed very strong to weak activities depending on the nature of the group (G) as follows:

(i) If G is an aliphatic acid derivative like **18a**, it achieved very strong activity against MCF-7 and strong activity against HepG-2.

(ii) However, if G is a benzoyl derivative like **19a**, it expressed strong activity towards MCF-7 and moderate activity towards HepG-2.

(iii) Besides, if G is an aliphatic ester derivative like **17a**, it showed moderate activity against MCF-7 and weak activity with HepG-2.

(iv) While, if G is an acetyl derivative like **20a**, it showed weak activity with both cell lines.

• Furthermore, the *N*-substituted pyrazole derivatives with CS-NH₂ side chain like **10a** and **10b** showed strong to moderate activities depending on the substituted phenyl ring attached to pyrazole as follow:

(i) In the case of the activated ring like 4-hydroxy benzene in compound **10a**, it showed moderate activities with both cell lines.

(ii) While, in the case of the deactivated ring like dichloro-benzene in compound **10b**, it showed strong activity on HepG-2 and moderate activity on MCF-7.

(b) Pyridine-based moieties:

• Pyridine analogs containing the NH₂ group in the alpha position to the attracting CN group like compounds **2a** and **6a** achieved very strong and strong activities against both cancer cell lines. The fused pyridopyridine derivative **6a** showed lower activities than the pyridine derivative **2a**.

• On the other hand, pyridines containing the OH group in the alpha position to the attracting groups (COCH₃, COOEt, and CN) in **3a**, **4a**, and **5a** compounds, respectively, showed moderate activities against the two cancer cell lines.

(c) Pyrimidine-based moieties:

• Pyrimidine derivatives (**11a** and **13a**) showed moderate and weak anticancer activities depending on the substitution in position 2 of pyrimidine as follows:

(i) If position 2 contains a donating group like NH₂ in compound **11a**, it showed moderate antitumor activities on both cancer cell lines.

(ii) While, when NH₂ functional group was condensed with the aromatic aldehyde like **13a**, the activity decreased on both cell lines.

2.2.2. EGFR and VEGFR-2 inhibitory activities. The superior anticancer candidates (**2a**, **6a**, **7a**, **10b**, **15a**, and **18a**) were selected to further evaluate their anti-EGFR and anti-VEGFR-2 potentialities (Fig. 3). All compounds showed very promising EGFR and VEGFR-2 μM inhibitory concentrations compared to erlotinib (0.037 μM) and sorafenib (0.034 μM), respectively. Notably, both **10b** and **2a** derivatives achieved the superior dual EGFR/VEGFR-2 inhibition with IC₅₀ values of (0.161 and 0.141 μM) and (0.209 and 0.195 μM), respectively. Besides, compounds (**6a**, **7a**, and **18a**) scored strong dual EGFR/VEGFR-2 inhibition with IC₅₀ values of (0.326 and 0.141 μM), (0.266 and 0.509 μM), and (0.436 and 0.344 μM), respectively. However, the least dual EGFR/VEGFR-2 inhibition was recorded for **15a** candidate with IC₅₀ values of 0.894 and 1.143 μM, respectively. Briefly, these μM inhibitory concentrations recommend greatly the proposed rationale design for the investigated compounds to act as promising dual EGFR/VEGFR-2 inhibitors.

2.2.3. Cell cycle analysis. The most active EGFR/VEGFR-2 inhibitor **10b** was further selected to evaluate the exact phase of cell cycle arrest. Herein, the most sensitive cell line (HepG2) was treated with the IC₅₀ value of **10b** (13.81 μM) to record its impact on the different phases of cell growth (% G0–G1, % S, and % G2/M). Compound **10b** showed a marked decline in cell populations at the S phase with 49.68% (1.37-fold) compared to that of the control (36.19%), Fig. 4.

2.2.4. Apoptosis analysis. Furthermore, the superior EGFR/VEGFR-2 inhibitor **10b** was selected to investigate the exact mechanism of cancer cell death whether it be due to apoptosis (programmed cell death) or necrosis (uncontrolled cell death). Therefore, the treatment of the HepG-2 cancer cell line with the IC₅₀ value of **10b** (13.81 μM) revealed an apparent increase in the total apoptosis percentage (from 1.75 to 44.26), compared to the control. This was accompanied by significant elevations in the percentage of the AnxV-FITC apoptotic cells in both the early



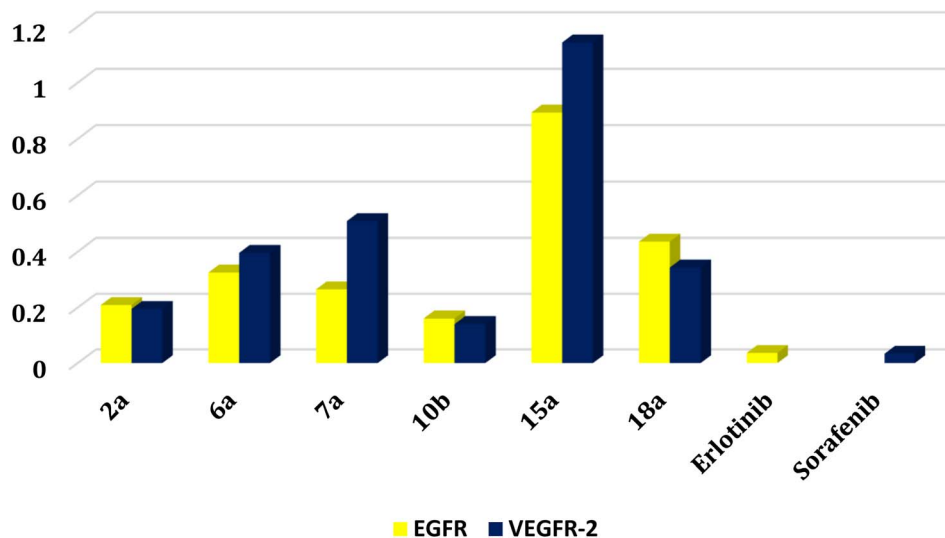
EGFR/VEGFR-2 (IC₅₀ uM)

Fig. 3 Effect of compounds (2a, 6a, 7a, 10b, 15a, and 18a) as dual EGFR/VEGFR-2 inhibitors.

DNA content

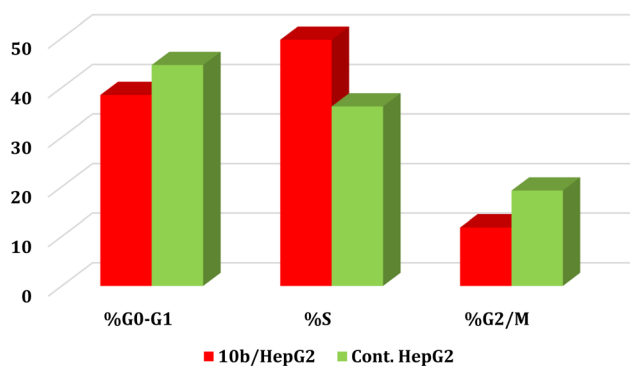


Fig. 4 Cell cycle analysis of HepG-2 cells treated with 10b at a concentration of 13.81 μ M.

(from 0.36 to 14.52%) and late (from 0.21 to 24.45%) apoptotic phases, compared to the control (Fig. 5 and 6). Accordingly, we can confirm the exact mechanism of the anticancer activity of 10b to be due to the programmed apoptosis pathway.

2.2.5. Antibacterial and antifungal activities. Using the inhibition zone approach and minimum inhibitory concentrations (MIC), all of the newly synthesized 4-thiophenyl-pyrazole, pyridine, and pyrimidine derivatives were tested for *in vitro* antibacterial and antifungal activities (Table 2). They were all tested against Gram-positive bacteria such as *Staphylococcus aureus* and *Bacillus subtilis* as well as Gram-negative bacteria such as *Escherichia coli* and *Pseudomonas aeruginosa*. Also, the antifungal activity was investigated against *Candida albicans* and *Aspergillus flavus* strains. Gentamycin was used as the standard antibacterial drug whereas ketoconazole was regarded as the primary antifungal one.

The findings of the antimicrobial test revealed that most of the investigated compounds exhibited strong to moderate antibacterial effects towards the Gram-positive and Gram-negative bacteria. With regards to the antifungal activity, all the synthesized compounds exhibited good activities against both *Candida albicans* and *Aspergillus fumigatus* except 1a, 1b, and 12a.

The antimicrobial activities based on the main nuclei (pyrazole-based, pyridine-based, and pyrimidine-based moieties) showed the following results:

(a) Pyrazole-based moieties

- Dihydropyrazole derivatives were more active than pyrazole derivatives. The NH-dihydropyrazole (7a) showed very strong activities with all six microbes.

- However, *N*-substituted dihydropyrazole showed activities from very strong to weak depending on the type of substituent as follows:

Apoptosis/Necrosis

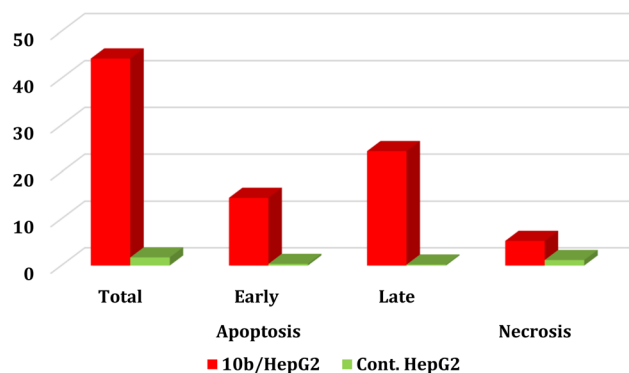


Fig. 5 Induction of apoptosis in HepG-2 cells by 10b shows both apoptotic (total, early, and late) and necrotic cell death.

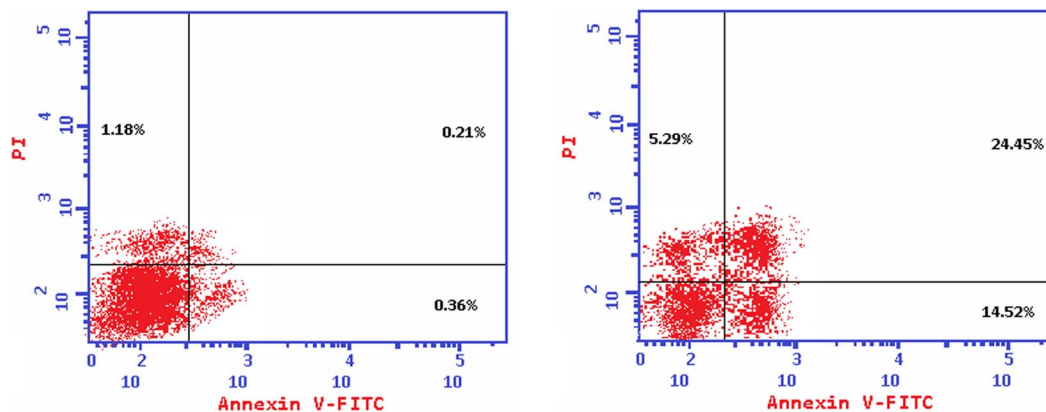


Fig. 6 Histograms of annexin-V apoptosis assay for **10b** in HepG-2 (lower right, upper right, lower left, and upper left represent early apoptotic, late apoptotic, viable, and necrotic phases, respectively).

Table 2 Antibacterial and antifungal activities of the newly designed 4-thiophenyl-pyrazole, pyridine, and pyrimidine derivatives

Comp.	Gram-positive bacteria				Gram-negative bacteria				Fungi			
	<i>S. aureus</i>		<i>B. subtilis</i>		<i>E. coli</i>		<i>P. aeruginosa</i>		<i>C. albicans</i>		<i>A. flavus</i>	
	Diameter of inhibition zone (mm)	% Activity index	Diameter of inhibition zone (mm)	% Activity index	Diameter of inhibition zone (mm)	% Activity index	Diameter of inhibition zone (mm)	% Activity index	Diameter of inhibition zone (mm)	% Activity index	Diameter of inhibition zone (mm)	% Activity index
1a	NA	—	NA	—	NA	—	NA	—	3	10.7	NA	—
1b	NA	—	NA	—	NA	—	NA	—	NA	—	NA	—
2a	10	55.5	15	68.2	9	42.8	12	63.1	18	64.3	12	46.1
2b	9	50.0	14	63.6	8	38.1	11	57.9	17	60.7	10	38.5
3a	5	27.8	9	40.9	4	19.0	6	31.6	11	39.3	10	38.5
4a	6	33.3	10	45.4	5	23.8	8	42.1	13	46.4	11	42.3
5a	6	33.3	10	45.4	5	23.8	10	52.6	14	50.0	8	30.8
6a	5	27.8	9	40.9	4	19.0	7	36.8	12	42.8	8	30.8
7a	15	83.3	19	86.4	12	57.1	17	89.5	23	82.1	18	69.2
8b	3	16.7	7	31.8	NA	—	4	21.0	9	32.1	5	19.2
9b	NA	—	6	27.3	NA	—	NA	—	8	28.6	3	11.5
10a	9	50.0	13	59.1	8	38.1	12	63.1	13	46.4	11	42.3
10b	12	66.7	17	77.3	9	42.8	13	68.4	20	71.4	14	53.8
11a	7	38.9	10	45.4	6	30.5	11	57.9	11	39.3	7	26.9
12a	NA	—	5	22.7	NA	—	3	15.8	6	21.4	NA	—
12b	7	38.9	12	54.5	5	23.8	8	42.1	15	53.6	10	38.5
13a	14	77.8	18	81.8	13	61.9	15	78.9	21	75.0	16	61.5
14a	4	22.2	8	36.4	3	14.3	6	31.6	7	25.0	5	19.2
15a	10	55.5	15	68.2	9	42.8	14	73.7	18	64.3	15	57.7
16a	8	44.4	11	50.0	7	33.3	11	57.9	15	53.6	12	46.1
17a	6	33.3	11	50.0	7	33.3	9	47.4	10	35.7	8	30.8
18a	13	72.2	17	77.3	10	47.6	15	78.9	20	71.4	16	61.5
19a	10	55.5	14	63.6	9	42.8	12	63.1	16	57.1	13	50.0
20a	3	16.7	6	27.3	NA	—	4	21.0	9	32.1	7	26.9
Gentamicin	18	100	22	100	21	100	19	100	—	—	—	—
Ketoconazole	—	—	—	—	—	—	—	—	28	100	26	100

(i) *N*-Substitution with CS-S-benzoyl like **18a** got moderate activity with *E. coli* and very strong activity with the other five tested microbes.

(ii) While *N*-substitution with CS-S-aliphatic acid like **19a** achieved moderate activities with all six microbes.

(iii) But other *N*-substituted dihydropyrazoles with CS-S-ester and CS-S-acetyl derivatives like **17a** and **20a** respectively showed weak activities with all the six tested microbes.

(iv) Moreover, *N*-substitution with CH₂-CO acquired strong to moderate activities based on the type of C=O; if *N*-

substituted with $\text{CH}_2\text{-CO}$ (ester) like **15a**, it showed strong activities with *B. subtilis*, *P. aeruginosa*, and *C. albicans*, and showed moderate activities with other tested microbes.

(v) While *N*-substitution with $\text{CH}_2\text{-CO}$ (amide) like **16a** showed weak activity with *E. coli* and moderate activities with the other five microbes.

- On the other hand, all pyrazole derivatives showed weak activities with all tested microbes except *N*-substituted pyrazole with CS-NH_2 like **10a** and **10b** achieved strong to moderate activities depending on the type of benzene derivative linked to position 3 of pyrazole:

(i) In the case of the activated ring like 4-hydroxyphenyl as in **10a**, it showed moderate activities with all tested microbes.

(ii) While, in the case of the deactivated ring like 3,4-dichlorophenyl as in **10b**, it showed very strong activity with *S. aureus*, *B. subtilis*, *P. aeruginosa*, and *C. albicans* and moderate activities with other tested microbes.

(b) Pyridine-based moieties

- Pyridine derivatives which contain NH_2 in the alpha position to N-heteroatom-like compounds **2a** and **2b** showed strong activities against *B. subtilis*, *P. aeruginosa*, and *C. albicans* and got moderate activities with the other tested microbes.

- However, pyridine derivatives that contain C=O in the alpha position to N-heteroatom as in compounds **3a–6a** showed weak activities against all tested microbes.

(c) Pyrimidine-based moieties

- Pyrimidine derivatives like **11a** and **13a** showed very strong to moderate activities depending on the type of substituent in position 2 of the pyrimidine ring, where:

(i) If position 2 contains a donating group like NH_2 as in **11a**, it showed very strong activity with *E. coli*, weak activity with *A. flavus*, and moderate activity with the other microbes.

(ii) While, when NH_2 condensed with aromatic aldehyde as in compound **13a**, it achieved very strong activities with all tested microbes.

2.3. In silico studies

2.3.1. Molecular docking studies. To understand the pattern by which the investigated compounds bound to the active site, all the newly synthesized candidates were subjected

to two different docking processes into the EGFR and VEGFR-2 binding sites. The affinities of the most active newly synthesized ligands (**2a**, **6a**, **7a**, **10b**, **15a**, and **18a**) toward the target proteins (Table 3) were compared according to the docking score values calculated using the MOE 2019.0102.⁴²

First, two validation processes were carried out to confirm the validity of the MOE program in getting accurate docking results. This was established by redocking each one of the two co-crystallized inhibitors (**HYZ** and **GIG**) of EGFR and VEGFR-2 receptors, respectively. The obtained low values of RMSD (0.99 and 1.29 Å, respectively) which represent the root mean square deviation between the native and redocked poses of the co-crystallized inhibitor ensured the valid performance.^{43,44} Besides, the most active dual EGFR/VEGFR-2 inhibitors (**2a** and **10b**) were selected for further investigations compared to the native inhibitors (**HYZ** and **GIG**) of EGFR and VEGFR-2, respectively (Table 4).

HYZ inside the binding pocket of the EGFR receptor ($S = -7.80 \text{ kcal mol}^{-1}$ and $\text{RMSD} = 1.33 \text{ Å}$) was found to form one π -cation bond with LYS745 at 4.16 Å and two π -H bonds with VAL726 at 4.29 and 4.64 Å, respectively. However, **GIG** inside the binding pocket of the VEGFR-2 receptor ($S = -9.54 \text{ kcal mol}^{-1}$ and $\text{RMSD} = 1.29 \text{ Å}$) formed two H-bonds with GLU833 at 2.90 and 2.79 Å, respectively, one H-bond with ASP1044 at 2.95 Å, and one π -H bond with LEU838 at 4.04 Å.

However, compound **2a** inside the binding pocket of the EGFR receptor ($S = -6.20 \text{ kcal mol}^{-1}$ and $\text{RMSD} = 1.44 \text{ Å}$) was found to form two H-bonds with MET793 and LYS745 amino acids at 3.16 and 3.74 Å, respectively. Besides, it formed two π -H bonds with LYS745 at 4.51 and 4.60 Å, and one π -H bond with VAL726 at 3.77 Å. On the other hand, its binding score within the active site of the VEGFR-2 receptor was $-6.08 \text{ kcal mol}^{-1}$ ($\text{RMSD} = 1.58 \text{ Å}$). It showed the formation of three H-bonds with GLU883, GLU915, and CYS917 at 3.04, 2.80, and 3.65 Å, respectively. It also bound LEU 838 with a π -H bond at 3.65 Å.

On the other hand, compound **10b** inside the binding pocket of the EGFR receptor ($S = -6.45 \text{ kcal mol}^{-1}$ and $\text{RMSD} = 1.42 \text{ Å}$) formed three H-bonds with ASN842, LEU788, and LYS745 amino acids at 3.12, 3.22, and 3.52 Å, respectively. Moreover, it formed a π -H bond with VAL726 at 3.82 Å. Furthermore, it showed the formation of one H-bond with ASP1044 at 2.92 Å and one π -H bond with VAL896 at 3.73 Å, within the active site of the VEGFR-2 receptor ($S = -6.44 \text{ kcal mol}^{-1}$ and $\text{RMSD} = 1.44 \text{ Å}$).

2.3.2. DFT calculations. From the experimental biological activity, compound **10b** showed very strong anti-proliferative activity against the two enzymes (EGFR and VEGFR-2) with IC_{50} values of 0.161 and 0.141 μM , respectively. The reference drug of EGFR (erlotinib) showed an IC_{50} of 0.037 μM while the reference drugs of VEGFR-2 (sorafenib) showed an IC_{50} value of 0.034 μM .

In the present section, we tried to correlate compound **10b** and the reference drugs, erlotinib, and sorafenib. Density functional theory (DFT) calculations were performed by using the Gaussian 09W program.⁴⁵ The optimized structures of **10b**, erlotinib, and sorafenib are represented in Fig. 7.

Table 3 Docking scores and RMSD values of the most biologically active compounds (**2a**, **6a**, **7a**, **10b**, **15a**, and **18a**) compared to **HYZ** and **GIG** inhibitors of EGFR and VEGFR-2 active sites, respectively

Compound	EGFR		VEGFR-2	
	Docking score (kcal mol^{-1})	RMSD	Docking score (kcal mol^{-1})	RMSD
2a	−6.20	1.44	−6.08	1.57
6a	−6.52	0.81	−6.01	1.47
7a	−5.88	1.15	−5.15	2.13
10b	−6.45	1.42	−6.44	1.44
15a	−6.96	1.98	−6.17	1.23
18a	−7.47	1.86	−6.86	1.62
HYZ	−7.81	0.99	—	—
GIG	—	—	−9.54	1.29



Table 4 2D and 3D pictures representing the interaction of compounds (2a and 10b) with EGFR and VEGFR-2 binding pockets, besides the docked co-crystallized inhibitors (HYZ and GIG)

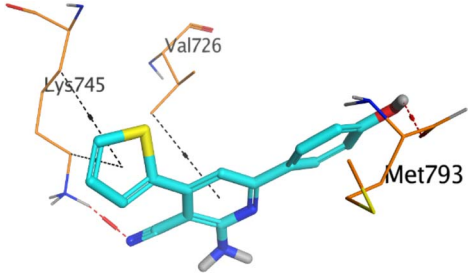
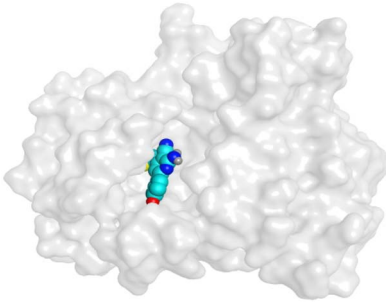
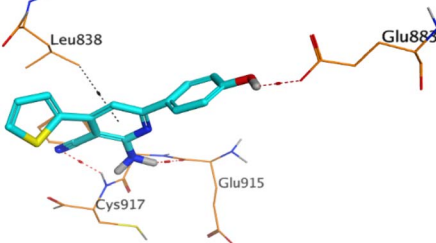
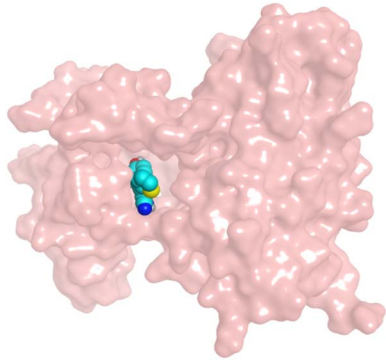
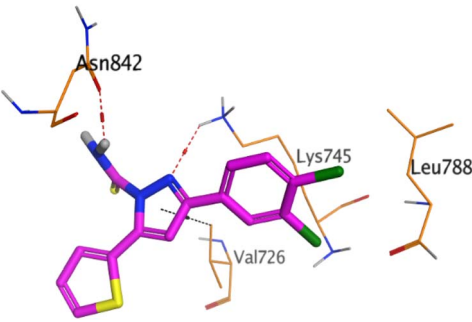
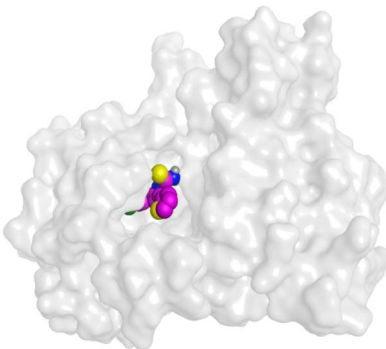
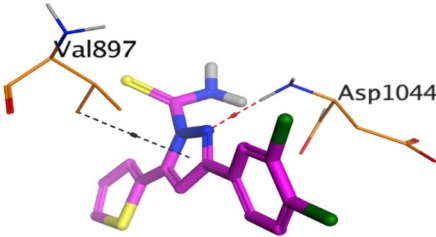
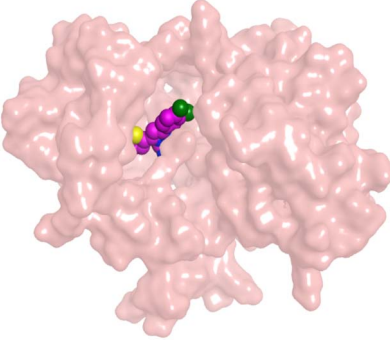
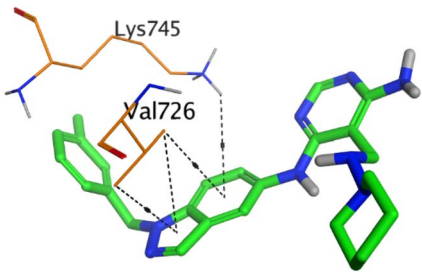
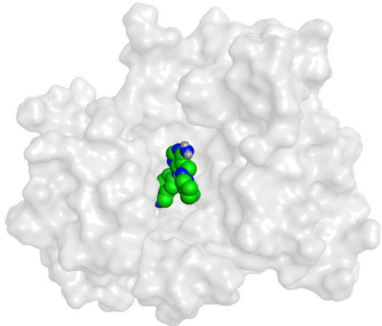
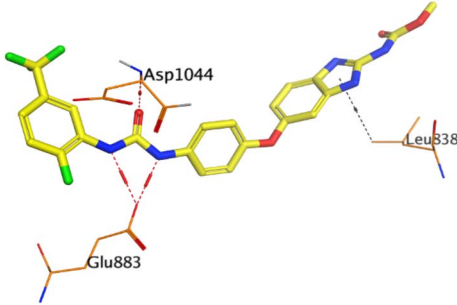
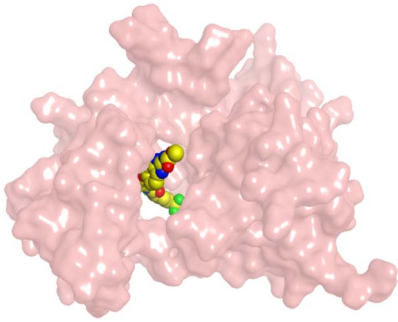
Compound	Receptor	3D interactions	3D positioning
2a	EGFR		
	VEGFR-2		
10b	EGFR		
	VEGFR-2		



Table 4 (Contd.)

Compound	Receptor	3D interactions	3D positioning
HYZ	EGFR		
GIG	VEGFR-2		

Moreover, the LUMO energy characterizes the sensitivity of the molecule to a nucleophilic attack, and the HOMO energy characterizes the susceptibility of a molecule to an electrophilic attack. Electronegativity (χ) is the parameter that reflects the ability of a molecule not to let out its electrons. Global softness (S) expresses the resistance of a system to the change in its number of electrons. The theoretical global parameters calculated at the same level of theory are listed in Table 5. The energy gap (E_g) between HOMO and LUMO characterizes the molecular chemical stability and molecular electrical transport properties because it is a measure of electron conductivity.

From the data in Table 5, the order of increasing E_{HOMO} is **10b** > sorafenib > erlotinib while the order of decreasing E_{LUMO} is erlotinib < sorafenib < **10b**. From the order of E_{HOMO} and E_{LUMO} , compound **10b** has the highest nucleophilicity and electrophilicity.

Also, analyzing the calculated values of hardness (η) and softness (S) for the investigated compounds revealed the donor-acceptor behavior of the studied molecules. Back to the energies of HOMO and LUMO, the order of increasing the energy gap is sorafenib > **10b** > erlotinib, so sorafenib is the hardest one (large energy gap) while erlotinib (small energy gap) represents the softest molecule (*c.f.* Fig. 7). Hence, the most polarizable (softest) with easier charge transfer and highest chemical reactivity molecule is erlotinib with $S = 0.238$ eV, while the least polarizable molecule (hardest) is sorafenib with $\eta = 2.279$ eV.

Moreover, the ionization potential (I) eV which is also related to the donating properties of the molecules (the higher the

ionization potential value the lower the donation ability of the molecule) was used to evaluate the tendency of molecules to be oxidized. It showed that the order of increasing of the most probable molecule to act as a reducing agent is erlotinib < sorafenib < **10b**.

Furthermore, the escaping tendency of an electron is measured by its chemical potential p (eV) and it is also related to its electronegativity. As p increases, the tendency of a molecule to lose an electron increases. Electronegativity (χ) represents the molecular ability to attract electrons, the (χ) values displayed in Table 5 show that **10b** > sorafenib > erlotinib in electronegativity and erlotinib > sorafenib > **10b** in chemical potential (P).

The chemical hardness and chemical potential are the main factors of the overall reactivity of the molecule and are the most fundamental descriptors of charge transfer during a chemical reaction.

2.4. Structure-activity relationship (SAR)

Following the biological studies of the new pyrazole, pyridine, and pyrimidine derivatives as anticancer and antimicrobial candidates, we can conclude the following interesting results (Fig. 8):

Generally, the 4-OH substitution on the side phenyl ring was found to be superior to the 3,4-diCl substitution regarding both the anticancer and antimicrobial activities.

- Regarding the anticancer activity: the descending order of activity was found to be (dihydropyrazole > *N*-substituted dihydropyrazole > pyridine > pyrimidine derivatives).



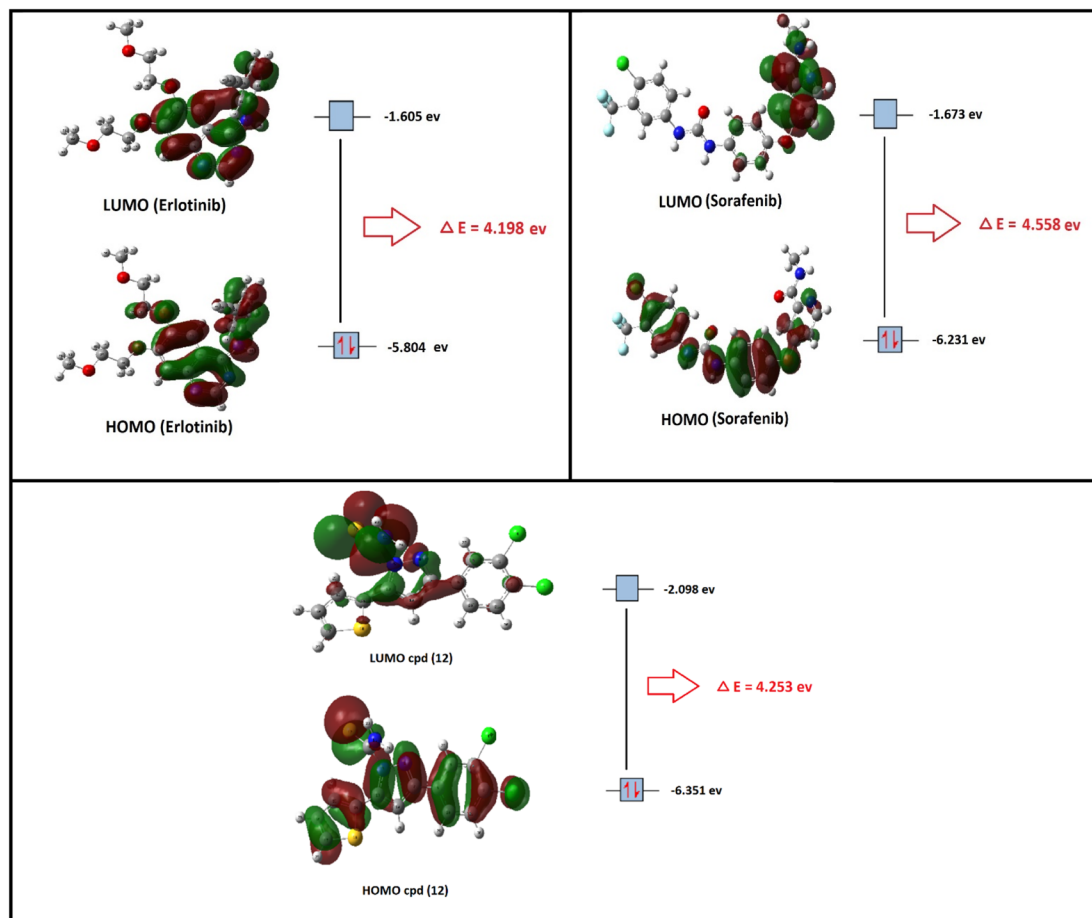


Fig. 7 The optimized structures and HOMO–LUMO charge density maps of compound **10b** and the reference drugs (erlotinib and sorafenib) were calculated at the B3LYP-6-31G+(d,p) level of theory.

Table 5 Total energy, the energy of HOMO and LUMO, energy gap, dipole moment, ionization potential (I , eV), electron affinity (A , eV), chemical hardness (η , eV), global softness (S , eV^{-1}), chemical potential (ρ , eV^{-1}), and electronegativity (χ , eV) of compound **10b** and the reference drugs (erlotinib and sorafenib) computed at the B3LYP/6-311+G(d,p) level of theory

Property	Compound		
	10b	Erlotinib	Sorafenib
E_{HOMO} (eV)	−6.351	−5.804	−6.231
E_{LUMO} (eV)	−2.098	−1.605	−1.673
Energy gap = $ E_{\text{HOMO}} - E_{\text{LUMO}} $ eV	4.253	4.198	4.558
Ionization potential ($I = -E_{\text{HOMO}}$) eV	6.351	5.804	6.231
Electron affinity ($A = -E_{\text{LUMO}}$) eV	2.098	1.605	1.673
Electronegativity $\chi = (I + A)/2$ eV	4.224	3.704	3.952
Chemical potential $\rho = -\chi$ eV	−4.224	−3.704	−3.952
Chemical hardness ($\eta = (I - A)/2$) eV	2.127	2.099	2.279
Chemical softness ($S = 1/2\eta$) eV	0.235	0.238	0.219

(i) Compound **7a** ($R^1 = -H$) with dihydropyrazole nucleus was found to be the most active against both HepG-2 and MCF-7 cancer cell lines.

(ii) However, the *N*-substituted dihydropyrazole derivatives achieved very strong to moderate antitumor activities according

to the R^1 substitution as follows: $-\text{CH}_2\text{COOC}_2\text{H}_5$ (**15a**) > $-\text{CH}_2-\text{CONHphSO}_2\text{NH}_2$ (**16a**) > $-\text{CSSCOPh}$ (**18a**) > $-\text{CSSCH}_2\text{COOH}$ (**19a**) > $-\text{CSSCH}_2\text{COOC}_2\text{H}_5$ (**17a**) > $-\text{CSSCOCH}_2\text{Cl}$ (**20a**) > $-\text{CSNH}_2$ (**10a**, **10b**).

(iii) Besides, the compounds containing the pyridine nucleus exhibited lower activity than the dihydropyrazole and *N*-substituted dihydropyrazole nuclei. The pyridine candidates showed very strong to moderate anticancer activities according to both R^2 and R^3 substituents as follows: $-\text{CN}$ and $-\text{NH}_2$ (**2a**) > fused pyridopyridine (**6a**) > $-\text{COCH}_3$ and $-\text{CO}$ (**3a**) \equiv $-\text{COOC}_2\text{H}_5$ and CO (**4a**) \equiv $-\text{CN}$ and $-\text{OH}$ (**5a**), respectively.

(iv) Moreover, the pyrimidine moiety derivatives were the lowest anticancer with moderate to weak activities regarding the R^4 substituent as follow: $-\text{NH}_2$ (**11a**) > $-\text{NCHphOH}$ (**13a**).

• Regarding the antimicrobial activity: the descending order of activity was noted to be (dihydropyrazole > *N*-substituted dihydropyrazole > pyrimidine > pyridine derivatives).

(i) Again, compound **7a** ($R^1 = -H$) with dihydropyrazole nucleus exhibited superior antibacterial and antifungal activities.

(ii) On the other hand, the *N*-substituted dihydropyrazole derivatives achieved strong to moderate antimicrobial activities according to the R^1 substitution as follows: $-\text{CSSCOPh}$ (**18a**) > $-\text{CSSCH}_2\text{COOH}$ (**19a**) > $-\text{CSSCH}_2\text{COOC}_2\text{H}_5$ (**17a**) > $-\text{CSSCOCH}_2\text{Cl}$ (**20a**) > $-\text{CSNH}_2$ (**10a**, **10b**).



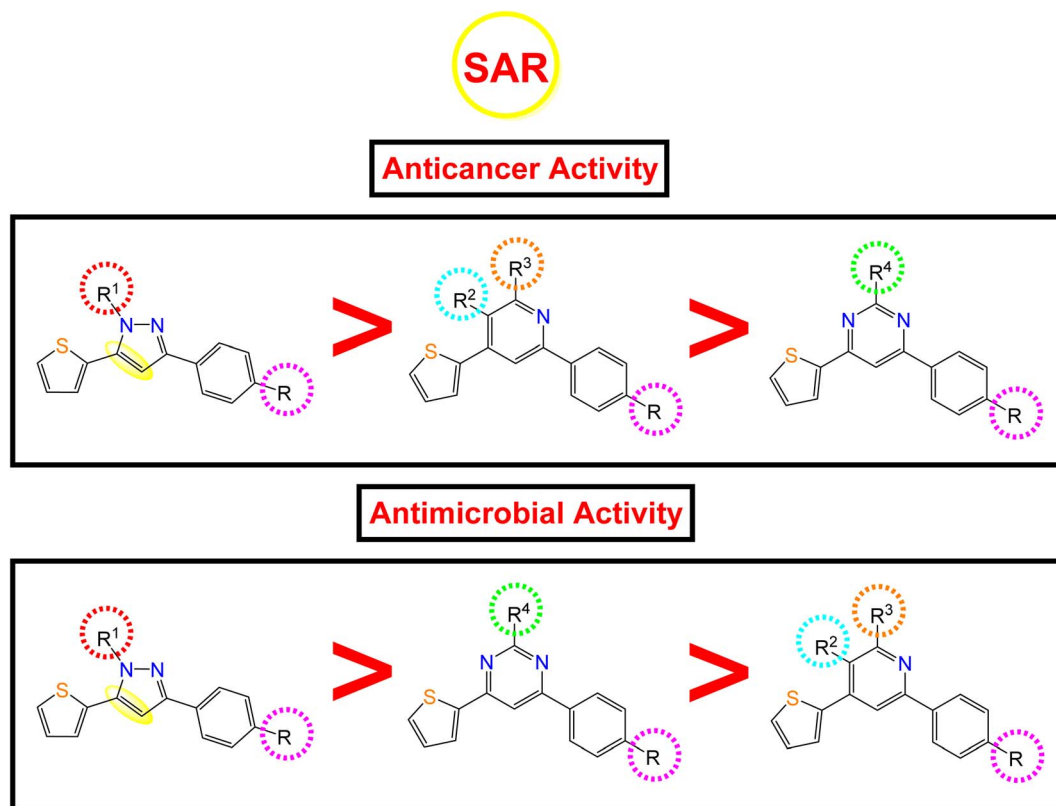


Fig. 8 Anticancer and antimicrobial activities of the novel pyrazole, pyridine, and pyrimidine candidates related to their chemical structures.

$\text{CH}_2\text{COOC}_2\text{H}_5$ (**15a**) > $-\text{CSSCH}_2\text{COOH}$ (**19a**) > $-\text{CSNH}_2$ (2,3-diClph) (**10b**) > $-\text{CSNH}_2$ (4-OHph) (**10a**) > $-\text{CH}_2\text{CONHphSO}_2\text{NH}_2$ (**16a**) > $-\text{CSSCH}_2\text{COOC}_2\text{H}_5$ (**17a**) > $-\text{CSSCOCH}_2\text{Cl}$ (**20a**).

(iii) Controversy, the pyrimidine moiety derivatives showed better antimicrobial activities than the pyridine ones. The order of decreasing the antimicrobial potentials was according to the R^4 substituent as follows: $-\text{NCHphOH}$ (**13a**) > $-\text{NH}_2$ (**11a**).

(iv) Furthermore, the pyridine-containing compounds exhibited lower antimicrobial activities according to both R^2 and R^3 substituents as follows: $-\text{CN}$ and $-\text{NH}_2$ (4-OHph) (**2a**) > $-\text{CN}$ and $-\text{NH}_2$ (2,3-diClph) (**2b**) > $-\text{CN}$ and $-\text{OH}$ (**5a**) > $-\text{COOC}_2\text{H}_5$ and CO (**4a**) > fused pyridopyridine (**6a**) > $-\text{COCH}_3$ and $-\text{CO}$ (**3a**).

3. Conclusion

Guided by the basic pharmacophoric requirements of both EGFR and VEGFR-2 inhibitors, novel twenty-two 4-thiophenyl-pyrazole, pyridine, and pyrimidine candidates were designed as potential dual EGFR/VEGFR-2 inhibitors. On the other hand, their antibacterial and antifungal activities were screened. First, the SAR studies revealed that the descending order of anticancer activity was according to (dihydropyrazole > *N*-substituted dihydropyrazole > pyridine > pyrimidine derivatives). The anticancer activities of compounds **2a**, **6a**, **7a**, **10b**, **15a**, and **18a** were found to be very strong to strong against both HepG-2 and MCF-7. These candidates were further evaluated against both EGFR and VEGFR-2 targets, compared to erlotinib and sorafenib, respectively. Both **10b** and **2a** derivatives

achieved better dual EGFR/VEGFR-2 inhibition with IC_{50} values of (0.161 and 0.141 μM) and (0.209 and 0.195 μM), respectively. Moreover, compound **10b** showed a marked decline in cell populations at the S phase with 49.68% (1.37-fold) compared to that of the control (36.19%). Also, the treatment of HepG-2 with the IC_{50} value of **10b** revealed significant elevations in the percentage of the AnxV-FITC apoptotic cells in both the early (from 0.36 to 14.52%) and late (from 0.21 to 24.45%) apoptotic phases, compared to the control. Accordingly, we can confirm the exact mechanism of the anticancer activity of **10b** to be due to apoptosis. On the other hand, screening the new compounds against Gram-positive bacteria, Gram-negative bacteria, and fungi revealed that most of them exhibited strong to moderate antibacterial and antifungal potentials. SAR studies showed that the descending order of antimicrobial activity was noted to be (dihydropyrazole > *N*-substituted dihydropyrazole > pyrimidine > pyridine derivatives). Collectively, compound **7a** with dihydropyrazole nucleus was found to be the most active against both HepG-2 and MCF-7 cancer cell lines and exhibited superior antibacterial and antifungal activities as well. Furthermore, both **2a** and **10b** showed greatly similar binding scores and modes regarding the co-crystallized inhibitors of EGFR and VEGFR-2 binding sites. Finally, the DFT calculations described that compound **10b** has the highest nucleophilicity and electrophilicity and the order of increasing the energy gap is sorafenib > **10b** > erlotinib, so sorafenib is the hardest one followed by **10b**.



4. Experimental section

4.1. Chemistry

All melting points were measured on a Gallen Kamp melting point apparatus (Sanyo Gallen Kamp, UK) and were uncorrected. The microwave reactions were done by Microsynth instrument type MA143 (micro wave flux). The ultrasound-assisted reactions were performed in Digital Ultrasonic Cleaner CD-4830 (35 kHz, 310 W). The IR spectra were recorded on a Pye-Unicam SP-3-300 infrared spectrophotometer (KBr disks) and expressed in wave number (cm^{-1}). ^1H NMR spectra were run at 300 and 400 MHz, on a Varian Mercury VX-300 and Bruker Avance III NMR spectrometer, respectively. TMS was used as an internal standard in deuterated dimethylsulphoxide ($\text{DMSO}-d_6$). Chemical shifts (δ) are quoted in ppm. The abbreviations used are as follows: s, singlet; d, doublet; m, multiplet. All coupling constant (J) values are given in hertz. Elemental analyses were performed on the CHN analyzer and all compounds were within ± 0.4 of the theoretical values. The reactions were monitored by thin-layer chromatography (TLC) using TLC sheets coated with UV fluorescent silica gel Merck 60 F254 plates and were visualized using a UV lamp and different solvents as mobile phases. All reagents and solvents were purified and dried by standard techniques. Compound **1a** was prepared according to the previously reported methodology.⁴⁶

4.1.1. Formation of (*E*)-1-(4-hydroxyphenyl)-3-(thiophen-2-yl)prop-2-en-1-one (1a**).** A mixture of 4-hydroxy acetophenone (1.36 g; 0.01 mol) and thiophene-2-carboxaldehyde (1.12 mL; 0.01 mol) in methanol (6 mL) and 10% sodium hydroxide solution (10 mL) was stirred at room temperature for 12 h. The reaction mixture was acidified with diluted hydrochloric acid the resulting solid was filtered out, dried, and recrystallized to produce compound **1a**.

4.1.2. Formation of (*E*)-1-(3,4-dichlorophenyl)-3-(thiophen-2-yl)prop-2-en-1-one (1b**).** A solution of 3,4-dichloro acetophenone (1.89 g; 0.01 mol) and thiophene-2-carboxaldehyde (1.12 mL; 0.01 mol) in ethanolic sodium hydroxide solution (20 mL) was stirred in an ice bath for 3 h. The obtained solid was filtered off and collected after recrystallization to give compound **1b**.

Yield 55%; as yellow crystal; mp 85 °C (EtOH); IR (cm^{-1}): 1655 ($\text{C}=\text{O}$); ^1H -NMR: 7.21 (d, d, 1H, CH thiophene ring), 7.57 (d, 1H, CH-olefinic), 7.73 (d, 1H, CH of benzene ring), 7.81 (s, 1H, CH benzene ring), 7.82 (d, 1H, CH of benzene ring), 7.92 (d, 1H, CH olefinic), 8.04 (d, 1H, CH of thiophene ring), 8.07 (d, 1H, CH of thiophene ring); MS (m/z) (%): 283 (M^+ , 15), 117 (100). Anal. calcd for $\text{C}_{13}\text{H}_8\text{Cl}_2\text{OS}$ (283.17): C, 55.14; H, 2.85; found: C, 54.89; H, 2.74.

4.1.3. General procedure for the synthesis of compounds (2a**) and (**2b**).** A mixture of chalcone **1a** (2.30 g; 0.01 mol) and/or chalcone (**1b**) (2.83 g; 0.01 mol), malononitrile (0.66 g; 0.01 mol) and ammonium acetate (2.31 g; 0.03 mol) was refluxed for 6–8 h in ethanol (20 mL). The reaction mixture was cooled and poured onto crushed ice, and the obtained solid was filtered off, dried, and recrystallized to give compounds **2a** and **2b**, respectively.

4.1.3.1. 2-Amino-6-(4-hydroxyphenyl)-4-(thiophen-2-yl)nicotinonitrile (2a**).** Yield 83%; orange crystal; mp 260 °C (EtOH);

IR (cm^{-1}): 3417 (OH), 3357, 3223 (NH_2), 2200 (CN), 1617 ($\text{C}=\text{N}$); ^1H -NMR: 6.86–8.00 (m, 7H, Ar-H), 7.15 (s, 2H, NH_2), 7.84 (s, 1H, CH of pyridine), 9.96 (s, 1H, OH). Anal. calcd for $\text{C}_{16}\text{H}_{11}\text{N}_3\text{OS}$ (293.34): C, 65.51; H, 3.78; N, 14.32; found: C, 65.36; H, 3.70; N, 14.21.

4.1.3.2. 2-Amino-6-(3,4-dichlorophenyl)-4-(thiophen-2-yl)nicotinonitrile (2b**).** Yield 63%; black crystal; mp 200 °C (EtOH); IR (cm^{-1}): 3362, 3238 (NH_2), 2213 (CN), 1640 ($\text{C}=\text{N}$); ^1H -NMR: 6.91 (s, 2H, NH_2), 6.94 (s, 1H, CH of pyridine ring), 7.19–7.92 (m, 6H, Ar-H). Anal. calcd for $\text{C}_{16}\text{H}_9\text{Cl}_2\text{N}_3\text{S}$ (346.23): C, 55.51; H, 2.62; N, 12.14; found: C, 55.34; H, 2.54; N, 12.21.

4.1.4. General procedure for the synthesis of compounds (3a**) and (**4a**).** A mixture of **1a** (2.30 g; 0.01 mol) and/or ethyl acetoacetate (1.30 mL; 0.01 mol) and diethyl malonate (1.60 mL; 0.01 mol) in presence of ammonium acetate (2.31 g; 0.03 mol) was refluxed for 8–10 h in ethanol (20 mL). After cooling, the reaction mixture was poured over ice, the obtained precipitate was filtered out, dried, and recrystallized to give **3a** and **4a**, respectively.

4.1.4.1. 3-Acetyl-6-(4-hydroxyphenyl)-4-(thiophen-2-yl)pyridin-2(1H)-one (3a**).** Yield 75%; brown crystal; mp 220 °C (EtOH) IR (cm^{-1}): 3331 (OH), 3107 (NH), 1695 ($\text{C}=\text{O}$); ^1H -NMR: 2.50 (s, 3H, $\text{CH}_3\text{-CO}$), 6.87–8.03 (m, 7H, Ar-H), 7.77 (s, 1H, CH pyridine ring), 9.86 (s, 1H, OH); MS (m/z) (%): 311 (M^+ , 20), 289 (100). Anal. calcd for $\text{C}_{17}\text{H}_{13}\text{N}_2\text{O}_3\text{S}$ (311.36): C, 65.58; H, 4.21; N, 4.50; found: C, 65.45; H, 4.14; N, 4.42.

4.1.4.2. Ethyl 6-(4-hydroxyphenyl)-2-oxo-4-(thiophen-2-yl)-1,2-dihydropyridine-3-carboxylate (4a**).** Yield 83%; brown crystal; mp 125 °C (EtOH); IR (cm^{-1}): 3170 (NH), 1725 (CO), 1675 (CO); ^1H -NMR: 1.11 (t, 3H, CH_3), 3.91 (q, 2H, CH_2), 6.79–8.01 (m, 7H, Ar-H), 7.19 (s, 1H, NH), 7.81 (s, 1H, CH pyridine ring), 9.95 (s, 1H, OH). Anal. calcd for $\text{C}_{18}\text{H}_{15}\text{N}_2\text{O}_4\text{S}$ (341.38): C, 63.33; H, 4.43; N, 4.10; found: C, 63.10; H, 4.32; N, 4.00.

4.1.5. Formation of 2-hydroxy-6-(4-hydroxyphenyl)-4-(thiophen-2-yl)nicotinonitrile (5a**).** A mixture of **1a** (2.30 g; 0.01 mol) and ethyl cyanoacetate (1.13 mL; 0.01 mol) in presence of ammonium acetate (2.31 g; 0.03 mol) was refluxed for 6–8 h in ethanol (20 mL). The reaction mixture was cooled and poured onto crushed ice/dilute hydrochloric acid and the formed product was filtered off, dried, and recrystallized to afford compound **5a**.

Yield 67%; yellow crystal; mp 200 °C (EtOH); IR (cm^{-1}): 3400 (OH), 2216 (CN), 1636 ($\text{C}=\text{N}$); ^1H -NMR: 6.81–8.01 (m, 8H, Ar-H), 10.22 (s, 1H, OH of benzene ring), 12.48 (s, 1H, OH of pyridine ring). Anal. calcd for $\text{C}_{16}\text{H}_{10}\text{N}_2\text{O}_2\text{S}$ (294.33): C, 65.29; H, 3.42; N, 9.52; found: C, 65.18; H, 3.48; N, 9.60.

4.1.6. Formation of 4-amino-7-(4-hydroxyphenyl)-2-oxo-5-(thiophen-2-yl)-1,2-dihydro-1,8-naphthyridine-3-carbonitrile (6a**)**

4.1.6.1. Conventional method. A mixture of chalcone **1a** (2.30 g; 0.01 mol), ethyl cyanoacetate (1.13 mL; 0.01 mol), and ammonium acetate (2.31 g; 0.03 mol) in ethanol (20 mL) was refluxed for 6–8 h, followed by addition of ethyl cyanoacetate (1.13 mL; 0.01 mol) and ammonium acetate (2.31 g; 0.03 mol) in ethanol (20 mL) with 6–8 h of continuous refluxing. The reaction mixture was cooled and poured onto crushed ice/dilute



hydrochloric acid and the formed product was filtered off, dried, and recrystallized to get compound **6a**.

4.1.6.2. Microwave method. A mixture of **1a** (2.30 g; 0.01 mol), ethyl cyanoacetate (2.26 mL; 0.02 mol), and ammonium acetate (2.31 g; 0.03 mol) in DMF (20 mL) was synthesized under microwave irradiation at 400 W for 6 min. The reaction mixture was poured onto crushed ice. The formed solid was filtered off, dried, and recrystallized to afford compound **6a**.

Yield 77%; yellow crystal; mp 260 °C (EtOH); IR (cm⁻¹) ν : 3480 (OH), 3369 (NH), 2217 (CN), 1683 (C=O), 1649 (C=N); ¹H-NMR: 6.47 (s, 2H, NH₂), 6.84–8.05 (m, 7H, Ar-H), 7.07 (s, 1H, CH of pyridine ring), 9.81 (s, 1H, NH), 12.51 (s, 1H, OH). Anal. calcd for C₁₉H₁₂N₄O₂S (360.39): C, 63.32; H, 3.36; N, 15.55; found: C, 63.09; H, 3.40; N, 15.48.

4.1.7. Formation of 4-(5-(thiophen-2-yl)-4,5-dihydro-1H-pyrazol-3-yl)phenol (7a). A mixture of chalcone **1a** (2.30 g; 0.01 mol) and hydrazine hydrate (2 mL) was refluxed for 8–10 h in ethanol (20 mL). After cooling, the reaction mixture was poured onto an ice bath, and the obtained precipitate was filtered out, dried, and recrystallized to get compound **7a**.

Yield 83%; white crystal; mp 100–102 °C (EtOH); IR (cm⁻¹) ν : 3290 (NH), 2879 (CH aliphatic), 1606 (C=N); ¹H-NMR: 2.82 (d, d, 2H, CH₂ of pyrazole ring), 5.05 (d, d, 1H, CH of pyrazole ring), 6.77–7.47 (m, 7H, Ar-H), 9.67 (s, 1H, NH). Anal. calcd for C₁₃H₁₂N₂OS (244.31): C, 63.91; H, 4.95; N, 11.47; found: C, 63.72; H, 4.84; N, 11.36.

4.1.8. Formation of 1-(3-(3,4-dichlorophenyl)-5-(thiophen-2-yl)-4,5-dihydro-1H-pyrazol-1-yl)ethan-1-one (8b). A mixture of **1b** (2.83 g; 0.01 mol) and hydrazine hydrate (2 mL) was refluxed for 3 h in presence of glacial acetic acid (15 mL). The obtained precipitate was cooled and poured onto crushed ice, filtered off, dried, and recrystallized to afford compound **8b**.

Yield 75%; brown crystal; mp 160 °C (EtOH); IR (cm⁻¹) ν : 2926 (CH-aliphatic), 1667 (CO), 1636 (C=N); ¹H-NMR: 2.48 (s, 3H, CH₃-CO), 3.27 (d, d, 2H, CH₂ of pyrazole ring), 5.84 (d, d, 1H, CH of pyrazole ring), 6.91–7.99 (m, 6H, Ar-H). Anal. calcd for C₁₅H₁₂Cl₂N₂OS (339.23): C, 53.11; H, 3.57; N, 8.26; found: C, 52.89; H, 3.50; N, 8.35.

4.1.9. Formation of 3-(3,4-dichlorophenyl)-1-phenyl-5-(thiophen-2-yl)-4,5-dihydro-1H-pyrazole (9b). A mixture of **1b** (2.83 g; 0.01 mol) and phenylhydrazine (1.08 g; 0.01 mol) was refluxed for 3 h in presence of ethanol (20 mL). Leave to cool, the solid obtained was filtered off, dried, and recrystallized from a suitable solvent to give compound **9b**.

Yield 81%; beige crystal; mp 130 °C (EtOH); IR (cm⁻¹) ν : 2867 (CH aliphatic), 1593 (C=N); NMR: 3.24 (d, d, 2H, CH₂ of pyrazole ring), 5.86 (d, 1H, CH of pyrazole ring), 6.75–7.93 (m, 11H, Ar-H). Anal. calcd for C₁₉H₁₄Cl₂N₂S (373.30): C, 61.13; H, 3.78; N, 7.50; found: C, 60.87; H, 3.66; N, 7.43.

4.1.10. Formation of 3-(4-hydroxyphenyl)-5-(thiophen-2-yl)-1H-pyrazole-1-carbothioamide (10a). A mixture of **1a** (2.30 g; 0.01 mol) and thiosemicarbazide (0.91 g; 0.01 mol) was refluxed for 18 h in presence of glacial acetic acid (5 mL) and ethanol (20 mL). The obtained precipitate was cooled and poured onto crushed ice, filtered off, dried, and recrystallized to get compound **10a**.

Yield 73%; green crystal; mp 195–197 °C (EtOH); IR (cm⁻¹) ν : 3406 (OH), 3343, 3268 (NH₂), 2921 (CH aliphatic), 1636 (C=N); ¹H-NMR: 7.37–8.51 (m, 7H, Ar-H), 6.88 (s, 1H, CH of pyrazole ring), 10.03 (s, 2H, NH₂), 10.42 (s, 1H, OH). Anal. calcd for C₁₄H₁₁N₃OS₂ (301.38): C, 55.79; H, 3.68; N, 13.94; found: C, 55.58; H, 3.72; N, 14.05.

4.1.11. Formation of 3-(3,4-dichlorophenyl)-5-(thiophen-2-yl)-1H-pyrazole-1-carbothioamide (10b). A mixture of **1b** (2.83 g; 0.01 mol) and thiosemicarbazide (0.91 g; 0.01 mol) in ethanolic sodium hydroxide solution (20 mL) was refluxed for 3 h. The reaction mixture was cooled, and acidified with diluted hydrochloric acid and the resulting solid was filtered out, dried, and recrystallized to afford compound **10b**.

Yield 65%; pale yellow crystal; mp 260 °C (EtOH); IR (cm⁻¹) ν : 3259, 3145 (NH₂), 1639 (C=N), 1596 (C=C), 1297 (C=S); ¹H-NMR: 6.22–8.17 (m, 6H, Ar-H), 6.99 (s, 1H, CH of pyrazole ring), 7.73 (s, 2H, NH₂); MS (*m/z*) (%): 354 (M⁺, 10), 109 (100). Anal. calcd for C₁₄H₉Cl₂N₃S₂ (354.27): C, 47.47; H, 2.56; N, 11.86; found: C, 47.30; H, 2.49; N, 11.76.

4.1.12. Formation of 4-(2-amino-6-(thiophen-2-yl)pyrimidin-4-yl)phenol (11a). A mixture of chalcone **1a** (2.30 g; 0.01 mol) and guanidine hydrochloride (0.95 g; 0.01 mol) in ethanolic sodium hydroxide solution (20 mL) was refluxed for 8 h. The reaction mixture was cooled, and acidified with diluted hydrochloric acid and the resulting solid was filtered out, dried, and recrystallized to afford compound **11a**.

Yield 76%; yellow crystal; mp 180 °C (EtOH); IR (cm⁻¹) ν : 3290 (OH), 3200 (NH₂), 1636 (C=N); ¹H-NMR: 6.91 (s, 2H, NH₂), 6.89–8.01 (m, 7H, Ar-H), 7.65 (s, 1H, CH of pyrimidine ring), 10.43 (s, 1H, OH); MS (*m/z*) (%): 269 (M⁺, 10), 74 (100). Anal. calcd for C₁₄H₁₁N₃OS (269.32): C, 62.44; H, 4.12; N, 15.60; found: C, 62.23; H, 4.19; N, 15.51.

4.1.13. Formation of 4-(1-(thiazolo[4,5-*b*]quinoxalin-2-yl)-5-(thiophen-2-yl)-1H-pyrazol-3-yl)phenol (12a). A solution of **10a** (3.03 g; 0.01 mol) and 2,3-dichloroquinoxaline (1.99 g; 0.01 mol) was refluxed for 15 h in presence of glacial acetic acid (5 mL) and absolute ethanol (20 mL). The obtained solid was filtered out, dried, and recrystallized to get compound **12a**.

Yield 78%; brown crystal; mp 250–252 °C (EtOH); IR (cm⁻¹) ν : 3444 (OH), 1664 (C=N); ¹H-NMR: 6.90–7.98 (m, 11H, Ar-H), 7.17 (s, 1H, CH of pyrazole ring), 9.00 (s, 1H, OH). Anal. calcd for C₂₂H₁₃N₅OS₂ (427.50): C, 61.81; H, 3.07; N, 16.38; found: C, 61.69; H, 3.00; N, 16.26.

4.1.14. Formation of compound 3-(3,4-dichlorophenyl)-N-(2-oxo-2-phenylethyl)-5-(thiophen-2-yl)-1H-pyrazole-1-carbothioamide (12b). A solution of **10b** (3.54 g; 0.01 mol) and phenacyl bromide (1.99 mL; 0.01 mol) was refluxed for 7–8 h in presence of acetic anhydride (20 mL), acetic acid (10 mL) and sodium acetate anhydrous (2 g). The obtained precipitate was cooled and poured onto crushed ice, filtered off, dried, and recrystallized to get compound **12b**.

Yield 63%; green crystal; mp 160 °C (EtOH); IR (cm⁻¹) ν : 3112 (NH), 2849 (CH aliphatic), 1668 (C=O), 1653 (C=N); ¹H-NMR: 4.82 (s, 2H, CH₂-C=O), 5.81 (s, 1H, NH), 6.85 (m, 11H, Ar-H), 6.86 (s, 1H, CH of pyrazole ring). Anal. calcd for C₂₂H₁₅Cl₂N₃-OS₂ (472.40): C, 55.94; H, 3.20; N, 8.90; found: C, 55.75; H, 3.12; N, 8.79.

4.1.15. Formation of (E)-2-(((4-(4-hydroxyphenyl)-6-(thiophen-2-yl)pyrimidin-2-yl)imino)methyl)phenol (13a). A mixture of **11a** (2.69 g; 0.01 mol) and salicylaldehyde (1.22 mL; 0.01 mol) with drops of piperidine was refluxed for 3 h in absolute ethanol (20 mL). The reaction mixture was cooled, and acidified with diluted HCl and the resulting solid was filtered out, dried, and recrystallized to give compound **13a**.

Yield 51%; brown crystal; mp 133–135 °C (EtOH); IR (cm⁻¹) ν : 3417 (OH), 1639 (C=N); ¹H-NMR: 6.84–8.02 (m, 11H, Ar-H), 7.51 (s, 1H, CH of pyrimidine ring), 7.56 (s, 1H, CH=N), 10.44 (s, 1H, OH), 10.44 (s, 1H, OH). Anal. calcd for C₂₁H₁₅N₃O₂S (373.43): C, 67.54; H, 4.05; N, 11.25; found: C, 67.39; H, 4.00; N, 11.34.

4.1.16. Formation of 3-(4-hydroxyphenyl)-N-phenyl-5-(thiophen-2-yl)-4,5-dihydro-1H-pyrazole-1-carbothioamide (14a). A mixture of **7a** (2.44 g; 0.01 mol) and phenyl isothiocyanate (1.35 mL; 0.01 mol) was refluxed for 10–12 h in the presence of benzene (20 mL) and drops of triethylamine. The obtained solid was filtered out, dried, and recrystallized to get compound **14a**.

Yield 81%; white crystal; mp 245–247 °C, EtOH; IR (cm⁻¹) ν : 3323 (OH), 3182 (NH), 3028 (CH aliphatic), 1604 (C=N); ¹H-NMR: 3.34 (d, d, 2H, CH of pyrazole), 3.83 (d, d, 1H, CH of pyrazole ring), 7.14–7.88 (m, 12H, Ar-H), 7.04 (s, 1H, NH), 10 (s, 1H, OH). Anal. calcd for C₂₀H₁₇N₃OS₂ (379.50): C, 63.30; H, 4.52; N, 11.07; found: C, 63.08; H, 4.59; N, 11.17.

4.1.17. Formation of ethyl 2-(3-(4-hydroxyphenyl)-5-(thiophen-2-yl)-4,5-dihydro-1H-pyrazol-1-yl)acetate (15a). A mixture of **7a** (2.44 g; 0.01) and ethyl chloroacetate (1.22 mL; 0.01 mol) was refluxed for 8 h in ethanolic sodium hydroxide solution (20 mL). The reaction mixture was cooled, and acidified with diluted hydrochloric acid and the resulting solid was filtered out, dried, and recrystallized to give compound **15a**.

Yield 75%; brown crystal; mp 65 °C, EtOH; IR (cm⁻¹) ν : 3254 (OH), 1731 (C=O), 1604 (C=N); ¹H-NMR: 1.02 (t, 3H, CH₃), 2.91 (s, 2H, CH₂), 3.59 (d, d, 2H, CH₂ of pyrazole ring), 3.93 (d, d, 1H, CH of pyrazole ring), 4.09 (q, 2H, CH₂), 6.77–7.99 (m, 7H, Ar-H), 10.44 (s, 1H, OH). Anal. calcd for C₁₇H₁₈N₂O₃S (330.40): C, 61.80; H, 5.49; N, 8.48; found: C, 61.65; H, 5.45; N, 8.57.

4.1.18. Formation of 2-(3-(4-hydroxyphenyl)-5-(thiophen-2-yl)-4,5-dihydro-1H-pyrazol-1-yl)-N-(4-sulfamoylphenyl)acetamide (16a). A mixture of **7a** (2.44 g; 0.01 mol) and 2-chloro-N-(4-sulfamoylphenyl)acetamide (2.48 g; 0.01 mol) was refluxed for 10–12 h in dioxane (20 mL) with drops of triethylamine. The reaction mixture was poured over ice, and the obtained precipitate was filtered out, dried, and recrystallized to get compound **16a**.

Yield 66%; brown crystal; mp 158–160 °C (EtOH); IR (cm⁻¹) ν : 3400 (OH), 3335, 3255 (NH₂), 3106 (NH), 2800 (CH aliphatic), 1694 (C=O), 1595 (C=N); ¹H-NMR: 3.06 (d, d, 2H, CH₂ of pyrazole), 3.90 (d, d, 1H, CH of pyrazole), 5.15 (s, 2H, CH₂), 6.72 (s, 2H, NH₂), 6.79–7.844 (m, 11H, H-Ar), 9.70 (s, 1H, NH), 10.80 (s, 1H, OH). Anal. calcd for C₂₁H₂₀N₄O₄S₂ (456.54): C, 55.25; H, 4.42; N, 12.27; found: C, 55.09; H, 4.33; N, 12.38.

4.1.19. General procedure for the synthesis of compounds (17a) (18a) (19a), and (20a). A mixture of **7a** (2.44 g; 0.01 mol) with anhydrous potassium carbonate (2.76 g; 0.02 mol),

tetrabutylammonium bromide (0.96 g; 0.003 mol), and carbon disulfide (10 mL) in ethanol (20 mL) was stirred for 15 min, then different alkyl halide namely ethylchloroacetate and chloroacetic acid and/or different acid chloride namely benzoyl chloride and chloroacetylchloride (0.01 mol) was added with 3 h of continuous stirring. The resulting solid was filtered out, dried, and recrystallized to give compounds **17a**, **19a**, **18a**, and **20a**, respectively.

4.1.19.1. Ethyl 2-((3-(4-hydroxyphenyl)-5-(thiophen-2-yl)-4,5-dihydro-1H-pyrazole-1-carbonothioyl)thio)acetate (17a). Yield 87%; yellow crystal; mp 200 °C (EtOH); IR (cm⁻¹) ν : 3258 (OH), 2974 (CH aliphatic), 1696 (C=O), 1607 (C=N); ¹H-NMR: 1.16 (t, 3H, CH₃), 3.14 (d, d, 2H, CH₂ of pyrazole), 3.39 (d, d, 1H, CH of pyrazole), 4.06 (s, 2H, CH₂), 4.08 (q, 2H, CH₂), 6.29–7.69 (m, 7H, Ar-H). Anal. calcd for C₁₈H₁₈N₂O₃S₃ (406.53): C, 53.18; H, 4.46; N, 6.89; found: C, 53.00; H, 4.38; N, 6.77.

4.1.19.2. Benzoic 3-(4-hydroxyphenyl)-5-(thiophen-2-yl)-4,5-dihydro-1H-pyrazole-1-carbothioic thioanhydride (18a). Yield 83%; yellow crystal; mp 240 °C EtOH; IR (cm⁻¹) ν : 3395 (OH), 1736–1696 (C=O), 1630 (C=N); ¹H-NMR: 3.14 (d, d, 2H, CH₂ of pyrazole ring), 3.69 (d, d, 1H, CH of pyrazole ring), 3.92 (s, 1H, OH), 6.73–8.14 (m, 12H, Ar-H); MS (*m/z*) (%): 424 (M⁺, 32), 360 (100). Anal. calcd for C₂₁H₁₆N₂O₂S₃ (424.55): C, 59.41; H, 3.80; N, 6.60; found: C, 59.24; H, 3.72; N, 6.71.

4.1.19.3. 2-((3-(4-Hydroxyphenyl)-5-(thiophen-2-yl)-4,5-dihydro-1H-pyrazole-1-carbonothioyl)thio)acetic acid (19a). Yield 81%; yellow crystal; mp 223–225 °C (EtOH); IR (cm⁻¹) ν : 3388 (OH), 2959 (CH aliphatic), 1692 (C=O), 1629 (C=N); ¹H-NMR: 3.14, 3.18 (d, d, 2H, CH₂ of pyrazole ring), 3.32 (d, d, 1H, CH of pyrazole ring), 3.60 (s, 2H, CH₂), 3.89 (s, 1H, OH), 6.84–7.67 (m, 7H, Ar-H), 8.80 (s, 1H, OH). Anal. calcd for C₁₆H₁₄N₂O₃S₃ (378.48): C, 50.78; H, 3.73; N, 7.40; found: C, 50.39; H, 3.55; N, 7.31.

4.1.19.4. 2-Chloroacetic-3-(4-hydroxyphenyl)-5-(thiophen-2-yl)-4,5-dihydro-1H-pyrazole-1-carbothioic thioanhydride (20a). Yield 83%; yellow crystal; mp 265 °C (EtOH); IR (cm⁻¹) ν : 3418 (OH), 2961 (CH aliphatic), 1746, 1694 (C=O), 1632 (C=N); ¹H-NMR: 3.14 (d, d, 2H, CH₂ of pyrazole ring), 3.60 (d, d, 1H, CH of pyrazole ring), 3.83 (s, 1H, OH), 4.35 (s, 2H, CH₂ acetyl chloride), 6.88–7.71 (m, 7H, Ar-H). Anal. calcd for C₁₆H₁₃ClN₂O₂S₃ (396.92): C, 48.42; H, 3.30; N, 7.06; found: C, 48.22; H, 3.22; N, 7.15.

4.2. Biological studies

4.2.1. Anti-proliferative activities. The antitumor activities of the newly synthesized derivatives against two cancer cell lines (HepG-2 and MCF-7). Both cell lines were purchased from ATCC (American Type Culture Collection) via the holding company for biological products and vaccines (VACSERA, Cairo, Egypt). The cytotoxicity was assessed using the SRB colorimetric assay.⁴⁷

4.2.2. EGFR and VEGFR-2 inhibitory activities. The superior anticancer candidates (**2a**, **6a**, **7a**, **10b**, **15a**, and **18a**) were selected to further evaluate their anti-EGFR and anti-VEGFR-2 potentialities based on a homogeneous luminescence release assay, as mentioned before.³⁴

4.2.3. Cell cycle analysis. The most active compound **10b** was further selected to evaluate the exact phase of cell cycle



arrest. Also, the most sensitive cell line (HepG2) was treated with the IC₅₀ value of **10b** (13.81 μ M) to record its impact on the different phases of cell growth (% G0–G1, % S, and % G2/M) using BD FACS Calibur flow cytometer.⁴⁸

4.2.4. Apoptosis analysis. The superior compound **10b** was selected to investigate the exact mechanism of cancer cell death whether it be due to apoptosis (programmed cell death) or necrosis (uncontrolled cell death). This was done using the FITC Annexin-V/PI kit.⁴⁹

4.2.5. Antibacterial and antifungal activities. Using the inhibition zone approach and minimum inhibitory concentrations (MIC), all of the newly synthesized 4-thiophenyl-pyrazole, pyridine, and pyrimidine derivatives were tested for *in vitro* antibacterial and antifungal activities.⁵⁰ They were all tested against Gram-positive bacteria such as *S. aureus* and *B. subtilis* as well as Gram-negative bacteria such as *E. coli* and *P. aeruginosa*. Also, the antifungal activity was investigated against *C. albicans* and *A. flavus* subtypes. Gentamycin was used as the standard antibacterial drug whereas ketoconazole was regarded as the primary antifungal one.

4.3. *In silico* studies

4.3.1. Molecular docking studies. Molecular docking studies are considered an influential method for the interpretation of molecular interactions between the synthesized compounds and the main amino acid residues at the specific binding site of the target receptor.^{51,52} The affinities of the newly synthesized ligands toward the target proteins (EGFR and VEGFR-2) were compared according to the docking score values calculated using the MOE 2019.0102.⁴²

All the newly synthesized 4-thiophenyl-pyrazole, pyridine, and pyrimidine derivatives were sketched using the ChemDraw and transferred to the MOE window, optimized for partial charges, and energy minimized as previously reported.⁵³ Then, the target two proteins (EGFR and VEGFR-2) were extracted from the PDB (IDs: 2RGP⁵⁴ and 2OH4 (ref. 55)), respectively. Each protein was corrected, 3D hydrogenated, and energy minimized as before.⁵⁶ Finally, two different docking processes were carried out to evaluate the binding affinities of the new candidates toward both EGFR and VEGFR-2 receptor pockets, respectively. The co-crystallized inhibitors were inserted as reference standards and the program specifications were adjusted as previously mentioned.⁵⁷

4.3.2. DFT calculations. Density functional theory (DFT) calculations were performed by using the Gaussian 09W program.⁴⁵ DFT calculations were carried out at the B3LYP level which is a combination with Becke's three-parameter (local, non-local, and Hartree–Fock) hybrid exchange functional with Lee–Yang–Parr correlation functional.^{58,59}

Full geometry optimization was performed using 6-31+G(d,p) as a basis set to generate the optimized structures and ground state properties of the studied compounds. The basis set 6-31+G(d,p) was augmented by 'd' polarization functions on heavy atoms and 'p' polarization functions on hydrogen atoms. Also, the diffuse functions for both hydrogen and heavy atoms were used.

To predict the chemical reactivity, some theoretical descriptors related to conceptual DFT have been determined for compound **10b** and reference drugs. The lowest unoccupied (vacant) molecular orbital (LUMO) energy (E_{LUMO}), the highest occupied molecular orbital (HOMO) energy (E_{HOMO}), the electronegativity (χ), the global softness (S), and hardness (η) descriptors were all determined from the optimized molecules. It should be noted that the descriptors related to frontier molecular orbitals FMO have been calculated in a very simple way in the context of the Koopmans approximation.⁶⁰

Author contributions

Conceptualization: A. A. A.-K., A. M. E.-N., and E. M. A.; data curation: S. M. A.-M., A. M. E.-N., A. K. A., N. E. A. A.-E.-S., and E. M. A.; visualization: A. A. A.-K. and E. M. A.; methodology: S. M. A.-M., A. A. A.-K., A. M. E.-N., and E. M. A.; validation: A. A. A.-K. and E. M. A.; supervision: A. A. A.-K., A. M. E.-N., and E. M. A.; writing – review & editing: S. M. A.-M., A. A. A.-K., A. M. E.-N., A. K. A., N. E. A. A.-E.-S., and E. M. A. Finally, all authors revised and approved the final submitted manuscript.

Conflicts of interest

The authors declared no conflict of interest.

References

- 1 C. Fitzmaurice, D. Dicker, A. Pain, H. Hamavid, M. Moradi-Lakeh, M. F. MacIntyre, C. Allen, G. Hansen, R. Woodbrook and C. Wolfe, *JAMA Oncology*, 2015, **1**, 505–527.
- 2 T. Al-Warhi, A. A. Al-Karmalawy, A. A. Elmaaty, M. A. Alshubramy, M. Abdel-Motaal, T. A. Majrashi, M. Asem, A. Nabil, W. M. Eldehna and M. Sharaky, *J. Enzyme Inhib. Med. Chem.*, 2023, **38**, 176–191.
- 3 W. Cao, H.-D. Chen, Y.-W. Yu, N. Li and W.-Q. Chen, *Chin. Med. J.*, 2021, **134**, 783–791.
- 4 E. Madbouly, E.-S. Lashine, A. A. Al-Karmalawy, M. Sebaiy, H. Pratsinis, D. Kletsas and K. Metwally, *New J. Chem.*, 2022, **46**, 22013–22029.
- 5 W. M. Eldehna, R. M. Maklad, H. Almahli, T. Al-Warhi, E. B. Elkaeed, M. A. Abourehab, H. A. Abdel-Aziz and A. M. El Kerdawy, *J. Enzyme Inhib. Med. Chem.*, 2022, **37**, 1227–1240.
- 6 T. Al-Warhi, M. M. Elbadawi, A. Bonardi, A. Nocentini, A. A. Al-Karmalawy, N. Aljaeed, O. J. Alotaibi, H. A. Abdel-Aziz, C. T. Supuran and W. M. Eldehna, *J. Enzyme Inhib. Med. Chem.*, 2022, **37**, 2635–2643.
- 7 A. Sabt, W. M. Eldehna, T. Al-Warhi, O. J. Alotaibi, M. M. Elaasser, H. Suliman and H. A. Abdel-Aziz, *J. Enzyme Inhib. Med. Chem.*, 2020, **35**, 1616–1630.
- 8 L. Akl, A. A. Abd El-Hafeez, T. M. Ibrahim, R. Salem, H. M. M. Marzouk, R. A. El-Domany, P. Ghosh, W. M. Eldehna and S. M. Abou-Seri, *Eur. J. Med. Chem.*, 2022, **243**, 114704.



- 9 L. K. Gediya and V. C. Njar, *Expert Opin. Drug Discovery*, 2009, **4**, 1099–1111.
- 10 W. M. Eldehna, M. A. El Hassab, M. F. Abo-Ashour, T. Al-Warhi, M. M. Elaasser, N. A. Safwat, H. Suliman, M. F. Ahmed, S. T. Al-Rashood and H. A. Abdel-Aziz, *Bioorg. Chem.*, 2021, **110**, 104748.
- 11 A. A. Gaber, A. M. El-Morsy, F. F. Sherbiny, A. H. Bayoumi, K. M. El-Gamal, K. El-Adl, A. A. Al-Karmalawy, R. R. Ezz Eldin, M. A. Saleh and H. S. Abulkhair, *Arch. Pharm.*, 2021, e2100258.
- 12 M. Khattab and A. A. Al-Karmalawy, *Future Med. Chem.*, 2021, **13**, 1623–1638.
- 13 C.-J. Tsai and R. Nussinov, *Semin. Cancer Biol.*, 2013, **23**(4), 235–242.
- 14 A. A. Elmaaty, K. M. Darwish, A. Chrouda, A. A. Boseila, M. A. Tantawy, S. S. Elhady, A. B. Shaik, M. Mustafa and A. A. Al-karmalawy, *ACS Omega*, 2022, **7**, 875–899.
- 15 R. R. Ezz Eldin, A. A. Al-Karmalawy, M. H. Alotaibi and M. A. Saleh, *New J. Chem.*, 2022, **46**, 9975–9984.
- 16 T. Al-Warhi, M. F. Abo-Ashour, H. Almahli, O. J. Alotaibi, M. M. Al-Sanea, G. H. Al-Ansary, H. Y. Ahmed, M. M. Elaasser, W. M. Eldehna and H. A. Abdel-Aziz, *J. Enzyme Inhib. Med. Chem.*, 2020, **35**, 1300–1309.
- 17 S. Sigismund, D. Avanzato and L. Lanzetti, *Mol. Oncol.*, 2018, **12**, 3–20.
- 18 M. H. Cohen, J. R. Johnson, Y. F. Chen, R. Sridhara and R. Pazdur, *Oncologist*, 2005, **10**, 461–466.
- 19 A. G. A. El-Helby, H. Sakr, I. H. Eissa, A. A. Al-Karmalawy and K. El-Adl, *Arch. Pharm.*, 2019, **352**, 1900178.
- 20 B. I. Rini, *Expert Opin. Pharmacother.*, 2006, **7**, 453–461.
- 21 D. N. Amin, D. R. Bielenberg, E. Lifshits, J. V. Heymach and M. Klagsbrun, *Microvasc. Res.*, 2008, **76**, 15–22.
- 22 C. Le Tourneau, S. Faivre and E. Raymond, *Cancer Treat. Rev.*, 2008, **34**, 37–48.
- 23 S. A. Wells Jr, J. E. Gosnell, R. F. Gagel, J. Moley, D. Pfister, J. A. Sosa, M. Skinner, A. Krebs, J. Vasselli and M. Schlumberger, *J. Clin. Oncol.*, 2010, **28**, 767.
- 24 W. M. Eldehna, M. A. El Hassab, Z. M. Elsayed, T. Al-Warhi, H. Elkady, M. F. Abo-Ashour, M. A. Abourehab, I. H. Eissa and H. A. Abdel-Aziz, *Sci. Rep.*, 2022, **12**, 12821.
- 25 M. M. Elbadawi, W. M. Eldehna, A. A. Abd El-Hafeez, W. R. Soma, A. Albohy, S. T. Al-Rashood, K. K. Agama, E. B. Elkaeed, P. Ghosh and Y. Pommier, *J. Enzyme Inhib. Med. Chem.*, 2022, **37**, 355–378.
- 26 Y. Ning, X. He, Y. Zuo, P. Cai, M. Xie, J. Wang and Y. Shang, *Adv. Synth. Catal.*, 2019, **361**, 3518–3524.
- 27 M. A. Hawata, W. A. El-Sayed, E. S. Nossier and A. A.-H. Abdel-Rahman, *Biointerface Res. Appl. Chem.*, 2022, **12**, 5217–5233.
- 28 A. Abo Elmaaty, M. I. A. Hamed, M. I. Ismail, E. B. Elkaeed, H. S. Abulkhair, M. Khattab and A. A. Al-Karmalawy, *Molecules*, 2021, **26**, 3772.
- 29 T. A. Farghaly, W. A. Al-Hasani and H. G. Abdulwahab, *Expert Opin. Ther. Pat.*, 2021, **31**, 989–1007.
- 30 N. M. Saleh, M. G. El-Gazzar, H. M. Aly and R. A. Othman, *Front. Chem.*, 2020, **7**, 917.
- 31 A. M. El-Naggar, A. Hassan, E. B. Elkaeed, M. S. Alesawy and A. A. Al-Karmalawy, *Bioorg. Chem.*, 2022, **123**, 105770.
- 32 C. B. Sangani, J. A. Makawana, X. Zhang, S. B. Teraiya, L. Lin and H.-L. Zhu, *Eur. J. Med. Chem.*, 2014, **76**, 549–557.
- 33 J. V. Faria, P. F. Vegi, A. G. C. Migueta, M. S. Dos Santos, N. Boechat and A. M. R. Bernardino, *Bioorg. Med. Chem.*, 2017, **25**, 5891–5903.
- 34 A. M. El-Naggar, A. M. A. Hassan, E. B. Elkaeed, M. S. Alesawy and A. A. Al-Karmalawy, *Bioorg. Chem.*, 2022, **123**, 105770.
- 35 A. M. El-Naggar, M. M. Hemdan and S. R. Atta-Allah, *J. Heterocycl. Chem.*, 2017, **54**, 3519–3526.
- 36 R. M. Mohareb, F. O. Al Farouk and W. W. Wardakhan, *Med. Chem. Res.*, 2018, **27**, 1984–2003.
- 37 R. Pluskota and M. Koba, *Mini-Rev. Med. Chem.*, 2018, **18**, 1321–1330.
- 38 C. N. Lakshmi, S. Balachandran, D. D. Arul, A. A. Ronaldo and J. I. Hubert, *Chem. Data Collect.*, 2019, **20**, 100205.
- 39 S. M. Batterjee, M. Marzouk, M. Aazab and M. El-Hashash, *Appl. Organomet. Chem.*, 2003, **17**, 291–297.
- 40 J. Makarevicius and V. Skaritis, *Heterocycles*, 1995, **41**, 1207.
- 41 H. M. Faidallah and M. S. Makki, *J. Chin. Chem. Soc.*, 1994, **41**, 585–589.
- 42 C. Inc., *Chemical Computing Group Inc.*, 2016, vol. 1010.
- 43 O. Kutkat, Y. Moatasim, A. A. Al-Karmalawy, H. S. Abulkhair, M. R. Gomaa, A. N. El-Taweel, N. M. Abo Shama, M. GabAllah, D. B. Mahmoud, G. Kayali, M. A. Ali, A. Kandeil and A. Mostafa, *Sci. Rep.*, 2022, **12**, 12920.
- 44 M. M. Hammoud, M. Khattab, M. Abdel-Motaal, J. Van der Eycken, R. Alnajjar, H. Abulkhair and A. A. Al-Karmalawy, *J. Biomol. Struct. Dyn.*, 2022, 1–18.
- 45 A. Frisch and USA Wallingford, *gaussian 09W Reference*, 2009, vol. 470, p. 25.
- 46 A. Al-Bogami, *Asian J. Chem.*, 2015, **27**, 4611–4614, DOI: [10.14233/ajchem.2015.19251](https://doi.org/10.14233/ajchem.2015.19251).
- 47 P. Skehan, R. Storeng, D. Scudiero, A. Monks, J. McMahon, D. Vistica, J. T. Warren, H. Bokesch, S. Kenney and M. R. Boyd, *J. Natl. Cancer Inst.*, 1990, **82**, 1107–1112.
- 48 K. L. Holmes, G. Otten and W. M. Yokoyama, *Curr. Protoc. Immunol.*, 2002, **49**, 5.4.1–5.4.22.
- 49 BD Biosciences, *Detection of Apoptosis Using the BD Annexin V FITC Assay on the BD FACSVerser™ System*, 2011, https://scholar.google.com/scholar?hl=en&as_sdt=0%2C5&q=B.+Biosciences%2C+2011&btnG=.
- 50 T. Al-Warhi, D. M. Elimam, Z. M. Elsayed, M. M. Abdel-Aziz, R. M. Maklad, A. A. Al-Karmalawy, K. Afarinkia, M. A. S. Abourehab, H. A. Abdel-Aziz and W. M. Eldehna, *RSC Adv.*, 2022, **12**, 31466–31477.
- 51 A. A. Elmaaty, W. M. Eldehna, M. Khattab, O. Kutkat, R. Alnajjar, A. N. El-Taweel, S. T. Al-Rashood, M. A. S. Abourehab, F. A. Binjubair, M. A. Saleh, A. Belal and A. A. Al-Karmalawy, *Int. J. Mol. Sci.*, 2022, **23**, 12235.
- 52 M. Elagawany, A. A. Elmaaty, A. Mostafa, N. M. Abo Shama, E. Y. Santali, B. Elgendy and A. A. Al-Karmalawy, *J. Enzyme Inhib. Med. Chem.*, 2022, **37**, 2112–2132.
- 53 A. A. Al-Karmalawy, M. S. Nafie, M. A. Shaldam, A. A. Elmaaty, S. A. Antar, A. A. El-Hamaky, M. A. Saleh,



- A. Elkamhawwy and H. O. Tawfik, *J. Med. Chem.*, 2023, **66**, 777–792.
- 54 G. Xu, M. C. Abad, P. J. Connolly, M. P. Neeper, G. T. Struble, B. A. Springer, S. L. Emanuel, N. Pandey, R. H. Gruninger and M. Adams, *Bioorg. Med. Chem. Lett.*, 2008, **18**, 4615–4619.
- 55 M. Hasegawa, N. Nishigaki, Y. Washio, K. Kano, P. A. Harris, H. Sato, I. Mori, R. I. West, M. Shibahara, H. Toyoda, L. Wang, R. T. Nolte, J. M. Veal and M. Cheung, *J. Med. Chem.*, 2007, **50**, 4453–4470.
- 56 R. F. Taher, A. A. Al-Karmalawy, A. I. Abd El Maksoud, H. Khalil, A. Hassan, E.-D. A. El-Khrisy and W. El-Kashak, *J. HerbMed Pharmacol.*, 2021, **10**, 443–458.
- 57 D. Elebeedy, I. Badawy, A. A. Elmaaty, M. M. Saleh, A. Kandeil, A. Ghanem, O. Kutkat, R. Alnajjar, A. I. Abd El Maksoud and A. A. Al-karmalawy, *Comput. Biol. Med.*, 2022, **141**, 105149.
- 58 M. Khattab and A. A. Al-Karmalawy, *Front. Chem.*, 2021, **9**, 628398.
- 59 A. A. Al-Karmalawy and M. Khattab, *New J. Chem.*, 2020, **44**, 13990–13996.
- 60 T. Koopmans, *Physica*, 1934, **1**, 104–113.

